Study the Effect of New Numerical and Analytical Solutions For Heat Irreversibility of Thermal Radiation and Ohmic Heating on Williamson Fluid

Ahmed R Khlefha*[1], Abeer M Jasim[2]
[1] *University of Sumer, Thi-Qar, Iraq.*
[2] *Department of Mathematics, College of Science, University of Basrah, Basrah, Iraq.*

Abstract:

   In this paper**,** a numerical and analytical treatment for the heat irreversibility of thermal radiation and Ohmic heating on the Williamson fluid problem is investigated with various physical parameters and the new initial conditions that pose arbitrary constants. The governing equations are transformed into dimensionless formulas, and the ordinary differential equations obtained are then solved using the BVP4c and the differential transform method (DTM). The heat irreversibility analysis is achieved by substituting the obtained results into entropy generation and Bejan number expressions. The results of numerical solutions are compared with the results of analytical solutions for various parameters. Fluid motion is reduced by the increasing values of the thermal radiation parameter, the magnetic parameter and the Reynolds number. In addition, it is worth noting that, except for the Weissenberg and Prandtl numbers, all of the flow parameters under investigation contribute to the augmentation of fluid temperature. Furthermore, it should be noted that the formation of entropy is heightened near the upper wall of the channel for all parameters, except for the magnetic field parameter.

Keywords: Williamson fluid, heat irreversibility, thermal radiation, inclined channel, differential transform method.

دراسة تأثير الحلول العددية والتحليلية الجديدة للانعكاس الحراري للإشعاع الحراري والتسخين الأومي على سائل ويليامسون

احمد رشيد* [1] ، عبير مجيد جاسم[2]
[1] جامعة سومر، ذي قار، العراق.
[2] قسم الرياضيات، كلية العلوم، جامعة البصرة، البصرة، العراق.

الخلاصة:

   في هذا البحث تم التحقيق في المعالجة العددية والتحليلية لعدم انعكاس الحرارة للإشعاع الحراري والتسخين الأومي على مشكلة مائع ويليامسون بمعايير فيزيائية مختلفة والظروف الأولية الجديدة التي تشكل ثوابت عشوائية. يتم تحويل المعادلات الحاكمة إلى صيغ بدون أبعاد ، ثم يتم حل المعادلات التفاضلية العادية

_____

*Email: a.rasheed@uos.edu.iq

التي تم الحصول عليها باستخدام BVP4c وطريقة التحويل التفاضلي (DTM). يتم إجراء تحليل عدم انعكاس

الحرارة عن طريق استبدال النتائج التي تم الحصول عليها في توليد إنتروبيا وتعبيرات أرقام بيجان. تمت مقارنة

نتائج الحلول العددية والتحليلية للمعلمات المختلفة. يتم تقليل حركة السوائل من خلال القيم المتزايدة لمعامل

الإشعاع الحراري والمعلمة المغناطيسية ورقم رينولدز. بالإضافة إلى ذلك ، فإن كل معلمة تدفق تم فحصها

تزيد من درجة حرارة السائل باستثناء معامل الإشعاع الحراري. تم تحسين توليد الانتروبيا أيضًا في الجدار

العلوي للقناة.

الكلمات المفتاحية: سائل ويليامسون ، عدم انعكاس الحرارة ، الإشعاع الحراري ، القناة المائلة ، طريقة

التحويل التفاضلي .

1. Introduction

Many scientists have recently become attracted to the study of viscous incompressible non-Newtonian fluids due to their numerous applications in engineering and industry. Newton's law of viscosity does not apply to non-Newtonian fluids. Numerous rheological models, including the Ellis, Power-law, Carreaus, Cross, and pseudoplastic fluids, have been proposed to overcome this problem since the Navier-Stokes equations alone are insufficient to reflect the rheological properties of these fluids. Pseudoplastic fluids are more important because they are used in many industries, like melting high-molecular-weight polymers, making photographic films, and extruding polymer sheets Williamson, [1],. Khan and Alzahrani [2] showed that the connection between velocity and the Weissenberg number is inverse. On the other hand, it gets better as the combined convection parameter rises. The Williamson flow of a stretching sheet was investigated by Nadeem et al [3]. As demonstrated by Hayat et al [4]. Thermal radiation, magnetic and electric fields, and two-dimensional Williamson fluid flow, all affect how the fluid moves. Krishnamurthy et al [5] explored the continuous flow of Williamson fluid in a horizontally stretched sheet with simultaneous melting heat transfer, chemical changes, and nanoparticles. Raza et al [6] studied hydromagnetic Williamson fluid under slip conditions. It was suggested that there was a direct correlation between the temperature profiles and the Williamson fluid parameter. Using the Keller box approach, Malik et al [7] examined the stretched cylinder using the Williamson fluid model. Al-Khafajy and Al-Delfi [8] conducted a study on the impact of an elastic wall on the peristaltic flow of Williamson fluid within two cylinders that are arranged concentrically. Monica et al [9] provided a method for analyzing the flow of non-Newtonian fluids across a stretching sheet at their stagnation points. Nagaraja and Reddy [10] introduced a model for Williamson fluids in two dimensions that flow via a cylinder. A study conducted by Khudair and Al-Khafajy [11] examined the impact of heat transfer on the magnetic oscillatory flow of a Williamson fluid through a porous material with two distinct geometric shapes, namely Poiseuille flow and Kuwait flow. Siddiqui et al [12] uncovered a method for analyzing Williamson fluid Blade coatings. Al-Khafajy [13] conducted a study on the peristaltic flow of Williamson fluid through a porous medium. The study focused on the combined impacts of magnetohydrodynamics (MHD) and wall characteristics, specifically the variable viscosity model. Shashikumar et al [14] examined the steady flow of Williamson fluid in a microchannel induced by viscous dissipation, magnetic effect, and Joule. Dissipation Readers who are interested in learning more about flow accounting for the viscoelastic shear-thinning features of non-Newtonian fluids should review the vast study. In [15,16], Ohmic heating is a sort of heating method in which heat is produced in fluid materials by electrical current. It results from the conversion of electrical energy to thermal energy, which is created by the applied electric field and fluid electrical resistance. Many academics have looked at difficulties with Newtonian and non-Newtonian fluid flow in the

context of Ohmic heating and heat transmission. The investigation of boundary layer flow, Ohmic heating, and chemical interaction with hydromagnetic heat transfer was carried out by Rao et al.[17] submitted that increasing values of Joule the temperature as well as the concentration distributions of the nanofluid are improved by the heating parameter. Prakash et al [18] examined the effects of a changing magnetic field on the mixed convective flow of an electrically charged nanofluid in a porous media. Furthermore, Muhammad et al [19] presented a study that examined the impact of chemical processes and viscosity dissipation on the electrical conductivity of Newtonian fluid flowing past an exponentially stretched sheet with ohmic heating. Adegbie et al [20] examined the effects of Joule heating and a field of magnets on airborne convection flow through a moving porous material. Numerous researchers have also studied the ohmic heating impact on non-Newtonian fluids. Goud and Nandeppanavar [21] conducted research on the impact of chemical processes and Ohmic heating on the hydromagnetic flow of a micropolar fluid. Hasan et al [22] analyzed the effects of a hall current with Ohmic heating is caused by waves of peristaltic in a non-Newtonian channel flow. Gireesha et al [23] studied cross-diffusion when examining the impact of Joule heating on Casson fluid hydromagnetic convection and mixed flow. Samuel and Olajuwon [24] examined the interactions between Joule heating, thermal radiation, Lorentz and forces of buoyancy in Maxwell fluid. Irreversibility analysis in gravity driven flows has applications in nature including wire drawing, spaying, fiberglass in metallurgical technology, the printing industry, during paper manufacturing processes, and the printing industry. Bejan [25] used the second law of thermodynamics to help understand how fluid generation of entropy rate and strategies for minimizing reversibility work. Furthermore, there have been reports of a Newtonian film flowing along a heated inclined plate by Saouli and Aboud-Saouli [26] with the intention of boosting the amount of energy available at work. Furthermore, researchers looked at the continuous, reactive flow of a pair stress fluid through a porous material Adesanya et al. [27] Adesanya and Makinde [28] investigated the entropy creation of third-grade fluid flow through a channel that is vertical and the effect of internal heat generation using the Adomian decomposition method. For more information see [29,32].In light of the significant uses of flow powered by gravitational force can be pointed the importance of the application as follows:
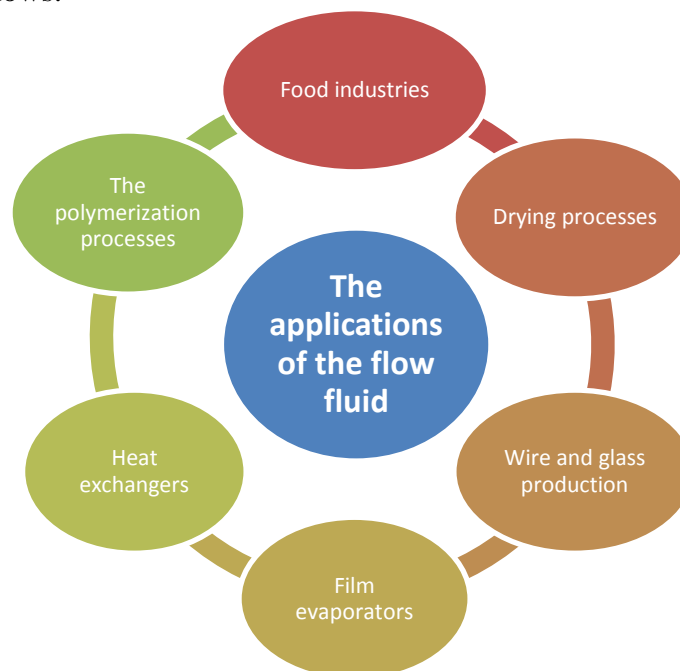
Figure.1: The application of the flow fluid.

In this paper, the heat irreversibility of thermal radiation and Ohmic heating on the Williamson fluid problem is resolved by using two methods BVP4c and DTM to find the numerical and analytical solutions respectively with a comparison between them. We have applied the differential transformation method, which is one of the most well-known and successful analytical techniques for dealing with nonlinear problems to find approximate-analytical solutions. DTM is an analytical method based on the Taylor series. It constructs an analytical solution in the form of a polynomial. Actually, DTM differs from the conventional high order Taylor series method, which calls for the algebraic computation of any necessary derivatives for the data functions. This method was initially used in the field of engineering by Zhang and Wang [33]. Numerous researchers chose to utilize this method to solve the nonlinear equations due to its advantages and capabilities. DTM is capable of solving any set of connected nonlinear equations. Khundu et al [34] utilized DTM and looked into the thermal analysis of exponential fins in the context of sensible and latent heat transfer. The DTM is applied to address the problem of heat transfers in the context of nanofluids and the outcomes are contrasted with those of the R-K approach by Usman et al [35]. Kanwal et al [36] investigated DTM analysis of MHD flow on a non-linear stretched sheet. Patel and Meher [37] analyzed the behavior of saturation profiles in fingers-imbibition processes during two-phase fluid flow through porous media and utilized it to calculate the solution of the Kolmogorov-Petrovskii-Piskunov equation. DTM was utilized by Yaghoobi and Torabi [38] to resolve nonlinear problems, the accuracy of their solutions was checked by comparing them to those obtained using the variational iteration method (VIM), homotopy perturbation method (HPM) and perturbation method (PM).

2. Governing Problem

The Williamson Magnetic flow is a fully advanced flow and also incompressible, where the fluid flows between two parallel and infinite panels at the distance of h, and it tends to an angle ε as shown in Figure2. The flow is along the $\bar{x}$ − axis whereas the $\bar{y}$ − axis is perpendicular to the flow in the Cartesian coordinates system approach. Transverse to the flow, a magnetic field of intensity $\mathcal{B}$ is applied. The magnetic Reynolds number is thought to be low and it is assumed that the physical quantities rely exclusively on $\bar{y}$, leading to a small induced magnetic field in comparison to the applied magnetic field. Furthermore, it is assumed that the electric field imparted is zero and that the hall effect is neglected. Using Boussinesq's approximation, the following set of equations describes the fluid motion, when hall currents ion-slip, thermoelectric effects and the electron pressure gradient are disregarded, Ohm's law for an electrically conductive fluid is:

$$\bar{J} = \sigma(\bar{E} + q\mathcal{B}) \tag{1}$$

where σ represents the fluid's electrical conductivity, $\bar{E}$ signifies the electric field vector, $\bar{J}$ is the current density vector, q is the velocity vector, and $\mathcal{B}$ is the magnetic field vector, the total magnetic field $\mathcal{B} = (\mathcal{B}_\circ + b)$. $\mathcal{B}_\circ$ and b respectively stand for the applied and produced magnetic fields. For tiny magnetic Reynolds numbers, the induced magnetic field is not taken into account. The energetic and momentum equations obtain the form [12] under the conditions given above.

$$\mathcal{v}_\circ \frac{d\bar{u}}{d\bar{y}} + \frac{d\bar{p}}{d\bar{x}} = \tilde{\alpha}\left(1 + \sqrt{2}\Sigma \frac{d\bar{u}}{d\bar{y}}\right)\frac{d^2\bar{u}}{d\bar{y}^2} + \rho g(\bar{T} - \bar{T}_1)\sin(\varepsilon) + \mathcal{B}_\circ J_z \tag{2}$$

$$\rho c_p \mathcal{v}_\circ \frac{d\bar{T}}{d\bar{y}} = \frac{\bar{\tau}(d^2\bar{T})}{d\bar{y}^2} + \tilde{\alpha}\left(1 + \frac{\Sigma}{\sqrt{2}}\frac{d\bar{u}}{d\bar{x}}\right)\left(\frac{d\bar{u}}{d\bar{x}}\right)^2 - \frac{d q_{\bar{r}}}{d\bar{y}} + \lambda\frac{J^2}{\sigma}, \tag{3}$$

For the purpose of including Joule dissipation, the index $\tilde{\lambda}$ is set to 1. Taking,

$$\bar{E}_{\bar{x}} = 0, \bar{E}_{\bar{z}} = 0 \text{, leads to } J_{\bar{x}} = 0, J_{\bar{x}} = -\rho B_\circ \bar{u}, \tag{4}$$

Eq. (2) and Eq. (3) are changed by the assumption of (4)

$$\rho v_{\circ} \frac{d\bar{u}}{d\bar{y}} + \frac{d\bar{p}}{d\bar{x}} = \tilde{\alpha}\left(1 + \sqrt{2}\Sigma\frac{d\bar{u}}{d\bar{y}}\right)\frac{d^2\bar{u}}{d\bar{x}^2} + \rho g(\bar{T} - \bar{T}_1)\sin(\varepsilon) - \rho B_{\circ}\bar{u}, \tag{5}$$

$$\rho c_p v_{\circ}\frac{d\bar{T}}{d\bar{y}} = \bar{\tau}\frac{d^2\bar{T}}{d\bar{y}^2} + \tilde{\alpha}\left(1 + \frac{\Sigma}{\sqrt{2}}\frac{d\bar{u}}{d\bar{x}}\right)\left(\frac{d\bar{u}}{d\bar{x}}\right)^2 - \frac{dq_{\bar{r}}}{d\bar{y}} + \lambda\rho B_{\circ}^2\bar{u}^2, \tag{6}$$

The boundary conditions are as follows:

$$\bar{u}(0) = 0, \bar{u}(h) = 0, \ \bar{T}(0) = \bar{T}_1, \ \bar{T}(h) = \bar{T}_2, \tag{7}$$

The Rosseland approximation is used to calculate the net radiative heat flux $q_{\bar{r}}$ for optically thick material.

$$q_{\bar{r}} = \frac{\rho^c}{3\bar{\tau}^c}\frac{d\bar{T}^4}{d\bar{y}} \qquad\qquad b \tag{8}$$

$\bar{T}^4$ being expanded in Taylor series about $\bar{T}_0$ as.

$$\bar{T'}^4 \cong \bar{T}_0^4 + 4\bar{T}_0^3(\bar{T} - \bar{T}_0) + 6\bar{T}_0^2(\bar{T} - \bar{T}_0)^2 + 4\bar{T}_0(\bar{T} - \bar{T}_0)^3, \tag{9}$$

and without accounting for the higher order components, if follows that

$$\bar{T'}^4 \cong \bar{T}_0^4 + 4\bar{T}_0^3\bar{T} + \bar{T}_0^3, \tag{10}$$

In light of equations (4) and (6), equation (3), we get

$$\rho c_p v_{\circ}\frac{d\bar{T}}{d\bar{y}} = \frac{\bar{\tau}(d^2\bar{T})}{d\bar{y}^2} + \tilde{\alpha}\left(1 + \frac{\Sigma}{\sqrt{2}}\frac{d\bar{u}}{d\bar{y}}\right)\left(\frac{d\bar{u}}{d\bar{y}}\right)^2 + \rho B_{\circ}^2\bar{u}^2 + \frac{16\rho^c\bar{T}^3}{3\bar{\tau}^c}\frac{d^2\bar{T}}{d\bar{y}^2}, \tag{11}$$

These similarity transformations are used to produce similarity equations.

$$\bar{u} = \frac{3\tilde{\alpha}}{\rho h}\mathcal{Y}(\xi), \xi = \frac{\bar{y}}{h} \text{ and }, \Phi = \frac{(\bar{T} - \bar{T}_1)}{(\bar{T}_2 - \bar{T}_1)}. \tag{12}$$

which yield

$$\left(1 + W_e\frac{d\mathcal{Y}(\xi)}{d\xi}\right)\frac{d^2\mathcal{Y}(\xi)}{d\xi^2} - R_e\frac{d\mathcal{Y}(\xi)}{d\xi} - M^2\mathcal{Y}(\xi) + G_{\bar{r}}\Phi\sin(\varepsilon) + \Omega = 0, \tag{13}$$

$$\left(1 + \frac{4}{3}R_a\right)\frac{d^2\Phi(\xi)}{d\xi^2} - R_eP_r\frac{d\Phi(\xi)}{d\xi} + E_cP_r\left(1 + \frac{W_e}{2}\frac{d\mathcal{Y}(\xi)}{d\xi}\right)\left(\frac{d\mathcal{Y}(\xi)}{d\xi}\right)^2 + M^2(\mathcal{Y}(\xi))^2 = 0. \tag{14}$$

giving the pertinent boundary conditions as

$$\mathcal{Y}(0) = 0, \mathcal{Y}(1) = 0, \Phi(0) = 1 \text{ and } \phi(1) = 0. \tag{15}$$

where,

$$R_e = \frac{v_{\circ}\rho h}{\tilde{\alpha}}, \Omega = \frac{\rho h^3}{\tilde{\alpha}^2}\left(-\frac{d\bar{p}}{d\bar{x}}\right), W_e = \frac{\tilde{\alpha}\sqrt{2}\Sigma}{\rho h^2}, M^2 = \frac{\rho h^2 B_{\circ}^2}{\tilde{\alpha}}, R_a = \frac{4\rho^c T_{\infty}^3}{\tau^c} \text{ and } G_r = \frac{\rho^2 h^3 \mathcal{B}(\bar{T}_2 - \bar{T}_1)}{\tilde{\alpha}}. \tag{16}$$
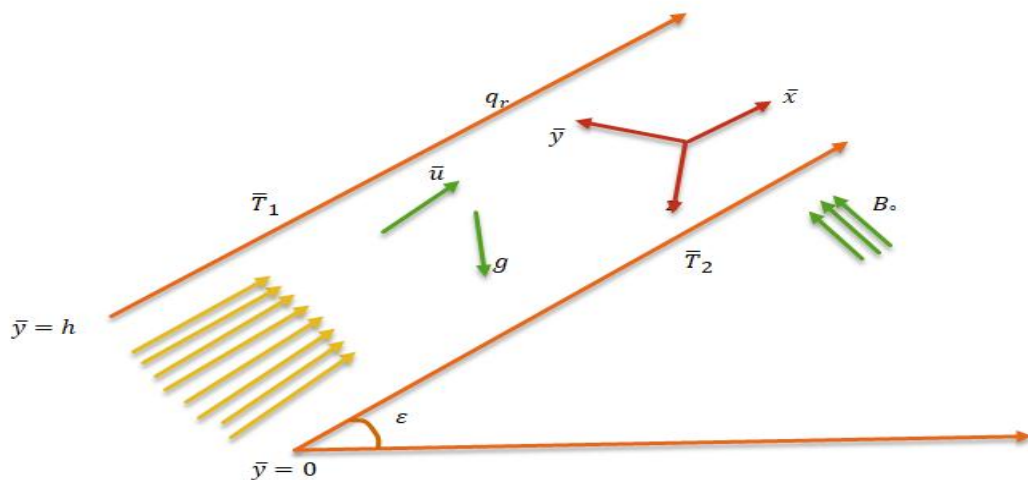
Figure 2: Schematic Diagram of the Problem.

3. The Ideal Basic of Differential Transform Method for Ordinary Differential Equations

In 1986, Zhou created the differential transformation method. The method was created to address initial value problems in the theory of electric circuits, both linear and non-linear. A semi-analytical method is based on Taylor series expansion. In using this strategy, we have put some transformation rules to use. The collection of basic equations is reduced to ODEs, and then these equations along with boundary conditions are converted using the DTM's prescribed procedures to produce the desired result. Basic definitions and operations of differential transformation are introduced for the function $\mathcal{Y}(\xi)$ as follows:

$$\mathcal{W}(k) = \frac{1}{\bar{k}!}\left(\frac{d^{\bar{k}}\mathcal{Y}(\xi)}{d\xi^{\bar{k}}}\right)_{\xi=\xi_0}, \tag{17}$$

where $\mathcal{Y}(\xi)$ is original function and $\mathcal{W}(k)$ is the transformed function. The inverse transform of the function $\mathcal{W}(k)$ gives,

$$\mathcal{Y}(\xi) = \sum_{k=0}^{\infty} \mathcal{W}(k)(\xi - \xi_0)^{\bar{k}}, \tag{18}$$

In actual applications, the function $\mathcal{Y}(\xi)$ is expressed by a finite series and Eq. (18) can be written as follows:

$$\mathcal{Y}(\xi) = \sum_{k=0}^{n} \mathcal{W}(k)(\xi - \xi_0)^{\bar{k}},$$

Substituting Eq. (17) into Eq. (18), gives

$$\mathcal{Y}(\xi) = \sum_{\bar{k}=0}^{n} \frac{(\xi-\xi_0)^{\bar{k}}}{\bar{k}!}\left(\frac{d^{\bar{k}}\mathcal{Y}(\xi)}{d\xi^{\bar{k}}}\right)_{\xi=\xi_0}, \tag{19}$$

New, the basic mathematical operations of differential transform that are commonly used are obtained and are listed in Table 1 as follows:

Table 1: The functions of differential Transformation

	Original function	Transformed function
1	$\mathcal{Y}(\xi) = t(\xi) \pm v(\xi)$	$\mathcal{W}(k) = T(k) \pm V(k)$
2	$\mathcal{Y}(\xi) = \epsilon t(\xi)$	$\mathcal{W}(k) = \epsilon T(k)$, ϵ is constant
3	$\mathcal{Y}(\xi) = t(\xi)v(\xi)$	$\mathcal{W}(k) = \sum_{i=0}^{\bar{k}} T(i)V(k-i)$
4	$\mathcal{Y}(\xi) = \dfrac{d^n t(\xi)}{d\xi^n}$	$\dfrac{(k+n)!}{k!}T(k+n)$

4. The Application of Differential Transform Method and BVP4c

In order to solve the thermal radiation and ohmic heating effects on the entropy generation of MHD Williamson fluid through an inclined channel, two schemes are implemented in this section: Namely, the differential transform method and BVP4c. These solutions, are approximate analytical and numerical solutions, and they can be summarized as follows:

4.1. Analytical Aspect

According to the differential transform method and Table.1 we obtain the iterative scheme for Eq. (13) and Eq. (14) given below:

$$(\bar{k}+1)\mathcal{W}(\bar{k}+2)(\bar{k}+2)$$
$$+ W_e \sum_{i=0}^{\bar{k}}\left((i+1)(i+2)\mathcal{W}(i+2)(1-i+\bar{k})\mathcal{W}(1-i+\bar{k})\right)-$$
$$R_e(\bar{k}+1)\mathcal{W}(\bar{k}+1) + G_r \sin(\varepsilon)\mathcal{V}(\bar{k}) + \delta(k)\Omega = 0, \tag{20}$$

$\left(1 + \frac{4R_a}{3}\right)(\bar{k} + 1)(\bar{k} + 2)\,\mathcal{V}(\bar{k} + 2) - E_c P_r(\bar{k} + 1)\mathcal{V}(\bar{k} + 1) + E_c P_r \sum_{i=0}^{\bar{k}}\big((i + 1)\mathcal{W}(i + 1)(1 - i + \bar{k})$

$\mathcal{W}(1 - i + \bar{k})\big) + \frac{E_c P_r W_e}{2}\sum_{j=0}^{\bar{k}}\sum_{i=0}^{\bar{k}-j}\big((j + 1)\mathcal{W}(j + 1)(\bar{k} + 1 - j)\mathcal{W}(\bar{k} + 1 - j)(\bar{k} + 1 - i - j)\,\mathcal{W}(\bar{k} + 1 - i - j)\big) = 0,$ (21)

The boundary conditions can be written as follows:

$\mathcal{W}(0) = 0 \,,\; \mathcal{W}(1) = \Pi \,,\; \mathcal{V}(0) = 1, \mathcal{V}(1) = \Lambda\,.$ (22)

Where Π and Λ can be determined using $\mathcal{Y}(1) = 0$ and $\phi(1) = 0$ and using the iterative of Eqs. (13)-(15) and we get approximants for $\mathcal{Y}$ and ϕ.

$\mathcal{Y}_1(\xi) = \Pi\xi,$

$\mathcal{Y}_2(\xi) = \Pi\xi - \left(\frac{G_r \sin(\varepsilon) - R_e a + \Omega}{2(aW_e + 1)}\right)\xi^2,$

$\mathcal{Y}_3(\xi) = \Pi\xi - \left(\frac{G_r \sin(\varepsilon) - R_e + \Omega}{2(aW_e + 1)}\right)\xi^2 - \frac{1}{6(aW_e + 1)^3}\,(\sin(\varepsilon)\,\Pi^2\Lambda \quad \psi G_r W_e^2 + \sin^2(\varepsilon)\,G_r^2 W_e +,$

$\qquad 2\Pi\Lambda \sin(\varepsilon)\,G_r W_e - \sin(\varepsilon)\,\Pi G_r R_e W_e + 2\Omega \sin(\varepsilon)\,G_r W_e - \Pi\Omega R_e W_e + \Omega^2 W_e + \Lambda G_r \sin(\varepsilon)$

$\qquad +\Pi\Omega R_e W_e + \Omega^2 W_e + \Pi G_r \sin(\varepsilon) + \sin(\varepsilon)\,G_r R_e - \Pi R_e^2 + \Omega R_e)\xi^3,$

The required approximate analytical solution of $\mathcal{Y}(\xi)$ is,

$\mathcal{Y}(\xi) = \Pi\xi - \left(\frac{G_r \sin(\varepsilon) - R_e \Pi + \Omega}{2(W_e + 1)}\right)\xi^2 - \frac{1}{6(aW_e + 1)^3}\,(\sin(\varepsilon)\,a^2 b G_r W_e^2 + \sin^2(\varepsilon)\,G_r^2 W_e +,$

$\qquad 2\Pi\Lambda \sin(\varepsilon)\,G_r W_e - \sin(\varepsilon)\,\Pi G_r R_e W_e + 2\Omega \sin(\varepsilon)\,G_r W_e - \Pi\Omega R_e W_e + \Omega^2 W_e + \Lambda G_r \sin(\varepsilon)$

$\qquad +\Pi\Omega R_e W_e + \Omega^2 W_e + \Pi G_r \sin(\varepsilon) + \sin(\varepsilon)\,G_r R_e - \Pi R_e^2 + \Omega R_e)\xi^3 + \cdots.$ (23)

And,

$\Phi_1(\xi) = 1 + \Lambda\xi,$

$\Phi_2(\xi) = 1 + \Lambda\xi + \frac{3\left(2R_e P_r - 2E_c P_r a^2 - a^3 W_e E_c P_r\right)}{4(3 + 4R_a)}\xi^2,$

$\Phi_3(\xi) =$

$1 + \Lambda\xi \quad + \quad \frac{3\left(2R_e P_r b - 2E_c P_r a^2 - a^3 W_e E_c P_r\right)}{4(3 + 4R_a)}\xi^2 + \frac{1}{6\left(1 + \frac{4R_a}{3}\right)}\left(\frac{R_e P_r\left(\Lambda R_e P_r - \Pi^2 E_c P_r \Pi^2 - \frac{1}{2}E_c P_r W_e \Pi^3\right)}{3 + 12R_a} + \right.$

$\left. \frac{2E_c P_r \Pi(G_r \sin(\varepsilon) - \Pi R_e + \Omega)}{\Pi W_e + 1} - \frac{\Lambda E_c P_r W_e(G_r \sin(\varepsilon) - \Pi R_e + \Omega)^2}{2(\Pi W_e + 1)^2} - \frac{2\Pi^2 E_c P_r W_e(G_r \sin(\varepsilon) - R_e \Pi + \Omega)}{2\Pi W_e + 1}\right)\xi^3,$

$\vdots$

The required approximate analytical solution of $\phi(\xi)$ is,

$\Phi(\xi) =$

$1 + \Lambda\xi \quad + \quad \frac{3\left(2R_e P_r \Lambda - 2E_c P_r \Pi^2 - a^3 W_e E_c P_r\right)}{4(3 + 4R_a)}\xi^2 + \frac{1}{6\left(1 + \frac{4R_a}{3}\right)}\left(\frac{R_e P_r\left(\Lambda R_e P_r - \Pi^2 E_c P_r \Pi^2 - \frac{1}{2}E_c P_r W_e \Pi^3\right)}{3 + 12R_a} + \right.$

$\left. \frac{2E_c P_r \Pi(G_r \sin(\varepsilon) - \Pi R_e + \Omega)}{\Pi W_e + 1} - \frac{\Lambda E_c P_r W_e(G_r \sin(\varepsilon) - \Pi R_e + \Omega)^2}{2(\Pi W_e + 1)^2} - \frac{2\Pi^2 E_c P_r W_e(G_r \sin(\varepsilon) - R_e \Pi + \Omega)}{2\Pi W_e + 1}\right)\xi^3 + \cdots$ (24)

4.2. Numerical Aspect

Eq. (13) and Eq. (14), which are nonlinear ordinary differential equations subject to Eq. (15) boundary conditions, are resolved using MATLAB's bvp4c solver. Other researchers have frequently utilized this algorithm to resolve the boundary value issue. A finite difference code with fourth order precision serves as the solution. The equations must be rewritten as a collection of equivalent first order ordinary differential equations in order to apply the solver.

From Eq. (13), we have

$\mathcal{Y}(\xi) = \mathcal{F}_1\,,\; \frac{d\mathcal{Y}(\xi)}{d\xi} = \mathcal{F}_2,\; \frac{d\mathcal{F}_2}{d\xi} = \frac{R_e y(2) + M y(1) + G_r y(3)\sin(\theta) + \Omega}{1 + W_e y(2)},$ (25)

From equation (14),

$$\phi(\xi) = \mathcal{F}_3 \,, \quad \frac{d\phi(\xi)}{d\xi} = \mathcal{F}_4 \,, \frac{d\mathcal{F}_4}{d\xi} = \frac{1}{\left(1+\frac{4}{3}R_a\right)}\left(R_e P_r y(4) - E_c P_r \left(1 + \frac{W_e}{2} y(2)\right) y(2)^2 - M y(1)^2\right).$$

(26)

From the boundary conditions (15), we obtain that

$$\mathcal{F}_1(0) = 0 \,, \ \mathcal{F}_1(1) = 0 \,, \ \mathcal{F}_3(0) = 1, \ \mathcal{F}_3(1) = 0.$$

(27)

Eqs. (25)-(27) have been numerically integrated into a predefined endpoint to create an initial value problem. The MATLAB package had to be used, which necessitated all these simplifications. With a 0.1 step size, this program is executed, and the range from 0 to 1 and back is then solved.

5. Convergence Test

In order to evaluate the errors of approximate analytical solutions to Eq.(13) and Eq.(14), we have applied the theorems from [39,40]. These theorems may be used to define the convergence condition, which is introduced as follows:

Definition 5.1: If there exists $0 \leq \pi_j < 1$ and $0 \leq \gamma_j < 1$ for $j = 0,1,2, ...$, then $\|\mathcal{W}_{j+1}\| \leq \pi_j \|\mathcal{W}_j\|$ and $\|\mathcal{V}_{j+1}\| \leq \gamma_j \|\mathcal{V}_j\|$ are the condition of convergent. Tables (2)-(5) show that the convergence criterion is satisfied for all solutions as follows:

Table 2: The values of convergent for $R_e = 1.5, \Omega = 0.1, W_e = 0.2 \,, G_r = 1, R_a = 0.2, Pr = 0.71, E_c = 0.5$ and $\varepsilon = \frac{\pi}{6}$

π_j	$M = 0.5$	$M = 0.75$	$M = 1$	γ_j	$M = 0.5$	$M = 0.75$	$M = 1$
π_0	0.000000000	0.000000000	0.000000000	γ_0	0.6014787155	0.636702430	0.63680712
π_1	0.851641566	0.8937669827	0.9354622132	γ_1	0.4281699754	0.4273627875	0.427016995
π_2	0.158529341	0.0978310728	0.0378859798	γ_2	0.2603940712	0.2615575953	0.261657342
π_3	0.161676139	0.2086863563	0.7494746125	γ_3	0.2403051562	0.2514764084	0.266814782
π_4	0.125534132	0.0300145311	0.0954303810	γ_4	0.1667845831	0.1188046782	0.059482599
⋮	⋮	⋮	⋮	⋮	⋮	⋮	⋮

Table 3: The values of convergent for $M = 0.5, \Omega = 0.1, W_e = 0.5 \,, G_r = 1, R_a = 0.1, Pr = 1, E_c = 0.5$ and $\varepsilon = \frac{\pi}{6}$

π_j	$R_e = 1$	$R_e = 1.5$	$R_e = 2$	γ_j	$R_e = 1$	$R_e = 1.5$	$R_e = 2$
π_0	0.000000000	0.000000000	0.000000000	γ_0	0.6205465619	0.479421642	0.36684652
π_1	0.962230062	0.8098068996	0.6783040315	γ_1	0.4550331254	0.6779697688	0.901050664
π_2	0.066893386	0.2100991668	0.3529045979	γ_2	0.2567776179	0.4162848567	0.569994683
π_3	0.225057339	0.1392890471	0.2888525746	γ_3	0.2894777510	0.3494639490	0.446284067
π_4	0.836012250	0.1538174316	0.1905400398	γ_4	0.1710042540	0.2739524325	0.358110075
⋮	⋮	⋮	⋮	⋮	⋮	⋮	⋮

Table 4: The values of convergent for $M = 0.5, \Omega = 0.1, W_e = 1, G_r = 1, R_e = 1, Pr = 0.71, E_c = 0.5$ and $\varepsilon = \frac{\pi}{6}$.

π_j	$R_a = 0.1$	$R_a = 0.5$	$R_a = 1$	γ_j	$R_a = 0.1$	$R_a = 0.5$	$R_a = 1$
π_0	0.000000000	0.000000000	0.000000000	γ_0	0.7175091456	0.800890731	0.85473003
π_1	0.955572731	0.9810938292	0.9972791474	γ_1	0.3212897536	0.2177403314	0.155247873
π_2	0.056286307	0.0280184309	0.0098506607	γ_2	0.1794522440	0.1158378785	0.077012123
π_3	0.073778332	0.1706627058	0.4333189367	γ_3	0.2361352592	0.2229821863	0.245699420
π_4	0.438337145	0.8294597679	0.6686008686	γ_4	0.08445922529	0.0040333507	0.061738902
$\vdots$	$\vdots$	$\vdots$	$\vdots$	$\vdots$	$\vdots$	$\vdots$	$\vdots$

Table 5: The values of convergent when $M = 0.75, \Omega = 0.1, G_r = 1, R_a = 0.3, Pr = 71, E_c = 0.5$ nd $\varepsilon = \frac{\pi}{6}$

π_j	$W_e = 0.1$	$W_e = 0.5$	$W_e = 1$	γ_j	$W_e = 0.1$	$W_e = 0.5$	$W_e = 1$
π_0	0.000000000	0.000000000	0.000000000	γ_0	0.5570893889	0.557080027	0.55706772
π_1	0.891036566	0.8668105950	0.8424373416	γ_1	0.5463053010	0.5462091422	0.546082655
π_2	0.115666021	0.1292530458	0.1419555973	γ_2	0.3342946212	0.3357522980	0.337242933
π_3	0.122627954	0.1966033467	0.2638231075	γ_3	0.3029172888	0.2985606926	0.294461338
π_4	0.533105616	0.0397480933	0.2036021039	γ_4	0.1950618042	0.1958012652	0.196205289
$\vdots$	$\vdots$	$\vdots$	$\vdots$	$\vdots$	$\vdots$	$\vdots$	$\vdots$

6. The Analysis of Validation

In order to validate the differential transform method, the exact solution of the Newtonian case W_e=0 is compared with the presented result of DTM in **Table (6)**. This table shows that the results show full agreement between the exact solution and DTM. The exact solution as presented by Makinde and Eegunjobi [36] as follows:

$$\mathcal{Y}(\xi) = \frac{\Omega\left(1 - \xi + \xi e^{R_e} - e^{\xi R_e}\right)}{R_e(e^{R_e} - 1)}, \tag{30}$$

The momentum of Equation (13) at $W_e = 0, G_r = 0, M = 0$, gives

$$\frac{d^2\mathcal{Y}(\xi)}{d\xi^2} + R_e \frac{d\mathcal{Y}(\xi)}{d\xi} + \Omega = 0, \tag{31}$$

The solution of the DTM of Equation (31) is written as

$$\mathcal{Y}(\xi) = a\xi + \left(\frac{aR_e - \Omega}{2}\right)\xi^2 - R_e\left(\frac{\Omega - aR_e}{6}\right)\xi^3 - R_e^2\left(\frac{\Omega - aR_e}{24}\right)\xi^4 - R_e^3\left(\frac{\Omega - aR_e}{120}\right)\xi^5 + \cdots \tag{32}$$

Table 6: The comparison of Exact, HPM and DTM solutions of Equations (13) at $Re = 1, \Omega = 1, W_e{=}0$
$G_r = 0$ and $M = 0$.

ξ	Exact [41]	HPM [36]	DTM
0.1	0.03879297	0.03879298	0.03879297
0.2	0.07114875	0.07114876	0.07114874
0.3	0.09639032	0.09639033	0.09639032
0.4	0.11376948	0.11376949	0.11376948
0.5	0.12245933	0.12245933	0.12245933
0.6	0.12154600	0.12154601	0.12154600
0.7	0.11001953	0.11001954	0.11001953
0.8	0.08676372	0.08676373	0.08676372
0.9	0.05054498	0.05054499	0.05054498

7. The Analysis of the Irreversibility

The values for temperature and velocity are used to compute the irreversibility rate inside the flow. In the presence of a magnetic field and thermal radiation, the equation for heat irreversibility is

$$\frac{\tau}{\overline{T}_1^2}\left(\frac{d\overline{T}}{d\bar{y}}\right)^2 + \frac{16\sigma^c\overline{T}^3}{3\tau^c}\left(\frac{d\overline{T}}{d\bar{y}}\right)^2 + \frac{1}{\overline{T}_1}\left(\tilde{\alpha}\left(1+\frac{\Sigma}{\sqrt{2}}\frac{d\overline{u}}{d\bar{x}}\right)\left(\frac{d\overline{u}}{d\bar{x}}\right)^2 - \sigma B_0^2 u^2\right) \tag{33}$$

Where, $\frac{\tau}{\overline{T}_1^2}\left(\frac{d\overline{T}}{d\bar{y}}\right)^2$ is heat transfer entropy generation, $\frac{16\sigma^c\overline{T}^3}{3\tau^c}\left(\frac{d\overline{T}}{d\bar{y}}\right)^2$ is the thermal radiation entropy generation, $\tilde{\alpha}\left(1+\frac{\Sigma}{\sqrt{2}}\frac{d\overline{u}}{d\bar{x}}\right)\left(\frac{d\overline{u}}{d\bar{x}}\right)^2$ is friction entropy generation and $\sigma B_0^2 u^2$ is magnetic field entropy generation . Applying the relations of the Eq. (16) yields the non-dimension form of Eq. (33).

$$\widetilde{N_s} = \left(1+\frac{4}{3}R_a\right)\left(\frac{d\Phi(\xi)}{d\xi}\right)^2 + E_c P_r L\left(\left(1+\frac{W_e}{2}\frac{dy(\xi)}{d\xi}\right)\left(\frac{dy(\xi)}{d\xi}\right)^2 - M^2\big(y(\xi)\big)^2\right), \tag{34}$$

Denoting,

$$\widetilde{N_1} = \left(1+\frac{4}{3}R_a\right)\left(\frac{d\Phi(\xi)}{d\xi}\right)^2 \text{ and } \widetilde{N_2} = E_c P_r L\left(\left(1+\frac{W_e}{2}\frac{dy(\xi)}{d\xi}\right)\left(\frac{dy(\xi)}{d\xi}\right)^2 - M^2\big(y(\xi)\big)^2\right) \tag{35}$$

Where, $\tilde{L} = \frac{\overline{T}_1}{T_2-T_1}$ and $\widetilde{N_s} = \frac{E_g\overline{T}_1^2 h^2}{\tau(T_2-T_1)}$. Then the Bejan number is represented as

$$Be = \frac{\widetilde{N_1}}{\widetilde{N_s}} = \frac{1}{1+\beta}, \quad \beta = \frac{\widetilde{N_1}}{\widetilde{N_2}}, \tag{36}$$

The expression is denoted by β is the distribution ratio of fluid irreversibility. The Bejan number can have any value in the range of 0 to 1. Especially, there are three cases for the Bejan number can be summarized as follows:

- $Be = 0$ irreversibility of fluid friction dominates.
- $Be = 1$ irreversibility of heat transfer predominates.
- $Be = 0.5$ both increase entropy production equally.

8. Results and Discussion

The impact of several physical parameters is examined for velocity ,temperature profiles in a range of $0.5 \leq R_a \leq 4.5, 0.1 \leq W_e \leq 1$, $G_r = 1, 0.5 \leq M \leq 1.5$,$0.71 \leq Pr \leq 7, 1.5 \leq R_a \leq 2.5,$ `$\pi/6 \leq \varepsilon \leq 7\pi/18$ and $1.5 \leq R_a \leq 2.5$. when $E_c = 0.5, \Omega = 1$ and $L = 1$,The comparison of the results for DTM with the numerical results generated using the BVP4c is provided in **Tables (8)– (17)**. These tables show that the results of DTM and the numerical solutions match well by finding the absolute errors. **Tables (11)-(17)** show the convergence of values Π and Λ that become similar in decimal places and are constant as continue to increment the iterative schemes. Also, the results of DTM and BVP4c are compared with the exact solution in Eq. (30) in **Table (18)**. This table shows the numerical solution close to the exact solution of the DTM results as the Reynolds number decreases.

Table 8: Comparison between DTM and BVP4c for $= 1.5, \Omega = 0.1, W_e = 0.5$, $G_r = 0.5, M = 0.5, R_a = 0.5$, $Pr = 0.71, E_c = 0.5$ and $\varepsilon = \frac{\pi}{6}$.

ξ	BVP4c		DTM		Errors	
	$\mathcal{Y}(\xi)$	$\Phi(\xi)$	$\mathcal{Y}(\xi)$	$\Phi(\xi)$	$Error_{y(\xi)}$	$Error_{\Phi(\xi)}$
0.0	0.00000000000	1.0000000000	0.00000000000	1.0000000000	0.000000	0.0000000
0.1	0.00974859363	0.9262739525	0.00973675964	0.9262590993	1.1×10^{-5}	1.4×10^{-5}
0.2	0.01761262044	0.8476652344	0.01758701087	0.8476343780	2.5×10^{-5}	3.0×10^{-5}
0.3	0.02350387485	0.7638581950	0.02346228968	0.7638100764	4.1×10^{-5}	4.8×10^{-5}
0.4	0.02732591013	0.6745147897	0.02726616814	0.6744484358	5.9×10^{-5}	6.6×10^{-5}
0.5	0.02897284594	0.5792729964	0.02889351382	0.5791884754	7.9×10^{-5}	8.4×10^{-5}
0.6	0.02832792897	0.4777450640	0.02897284594	0.4776447706	6.4×10^{-4}	1.0×10^{-4}
0.7	0.02526175503	0.3695155589	0.02832792897	0.3694062296	3.0×10^{-3}	1.0×10^{-4}
0.8	0.01963002253	0.2541391745	0.02526175503	0.2540348714	5.6×10^{-3}	1.0×10^{-4}
0.9	0.01127064349	0.1311382570	0.01963002253	0.1310646039	8.3×10^{-3}	7.3×10^{-5}
1.0	0.00000000000	0.0000000000	0.00000000000	0.0000000000	0.0000000	0.0000000

Table 9: Comparison between DTM and BVP4c for $Re = 1, \Omega = 0.3, W_e = 0.2$, $G_r = 1, M = 1, R_a = 0.1$
$Pr = 1, E_c = 0.5$ and $\varepsilon = \frac{\pi}{6}$.

ξ	BVP4c		DTM		Errors	
	$\mathcal{Y}(\xi)$	$\Phi(\xi)$	$\mathcal{Y}(\xi)$	$\Phi(\xi)$	$Error_{y(\xi)}$	$Error_{\Phi(\xi)}$
0.0	0.00000000000	1.0000000000	0.00000000000	1.0000000000	0.00000000	0.00000000
0.1	0.02371956138	0.9354330563	0.02371003187	0.9351751224	5.2×10^{-6}	2.5×10^{-4}
0.2	0.04233341495	0.8644816485	0.04231387503	0.8641478544	1.9×10^{-5}	3.3×10^{-4}
0.3	0.05581881724	0.7869547563	0.05578957312	0.7864253221	2.9×10^{-5}	5.2×10^{-4}
0.4	0.06403146075	0.7021901453	0.06409372918	0.7024484968	6.2×10^{-5}	2.5×10^{-4}
0.5	0.06710473321	0.6085516546	0.06716077345	0.6085937577	5.6×10^{-5}	4.2×10^{-5}
0.6	0.06494898975	0.5083243982	0.06490223108	0.5081744538	4.6×10^{-5}	1.4×10^{-4}
0.7	0.05725085462	0.3967076456	0.05720598944	0.3964424658	4.4×10^{-5}	2.6×10^{-4}
0.8	0.04397258698	0.2768050907	0.04393556598	0.2765897697	3.7×10^{-5}	2.1×10^{-4}
0.9	0.02495156862	0.1446121667	0.02492937590	0.1447499975	2.2×10^{-5}	1.3×10^{-4}
1.0	0.00000000000	0.0000000000	0.00000000000	0.0000000000	0.00000000	0.00000000

Table 10: Comparison between DTM and BVP4c for $Re = 1, \Omega = 0.1, W_e = 1, G_r = 1, M = 1.5, R_a = 0.2$
$Pr = 0.71, E_c = 0.5$ and $= \frac{\pi}{6}$.

	BVP4c		DTM		Errors	
ξ	$\mathcal{Y}(\xi)$	$\Phi(\xi)$	$\mathcal{Y}(\xi)$	$\Phi(\xi)$	$Error_{\mathcal{Y}(\xi)}$	$Error_{\Phi(\xi)}$
0.0	0.00000000000	1.0000000000	0.00000000000	1.0000000000	0.00000000	0.00000000
0.1	0.01452225341	0.9234397975	0.01450520569	0.9232785625	1.7×10^{-5}	1.6×10^{-4}
0.2	0.02547887855	0.8424109662	0.02544300228	0.8420763349	3.5×10^{-5}	3.3×10^{-4}
0.3	0.03303406570	0.7566722420	0.03297779151	0.7561514443	5.6×10^{-5}	5.2×10^{-4}
0.4	0.03733202925	0.6659597131	0.03725424309	0.6652445103	7.7×10^{-5}	7.1×10^{-4}
0.5	0.03849625427	0.5699895100	0.03839688559	0.5690848017	9.9×10^{-5}	9.0×10^{-4}
0.6	0.03662871283	0.4684593154	0.03650969693	0.4673963905	6.4×10^{-4}	1.0×10^{-3}
0.7	0.03180729013	0.3610475920	0.03167569524	0.3599043086	1.1×10^{-3}	1.1×10^{-3}
0.8	0.02408468418	0.2474132890	0.02395652956	0.2463407018	1.3×10^{-3}	1.0×10^{-3}
0.9	0.01348553282	0.1271937712	0.01339207011	0.1264509855	1.2×10^{-5}	7.4×10^{-4}
1.0	0.00000000000	0.0000000000	0.00000000000	0.0000000000	0.00000000	0.00000000

Table 11: The convergent of $\frac{d\mathcal{Y}(0)}{d\xi}$ between DTM and BVP4c.

M	BVP4c	DTM	Re	BVP4c	DTM
0.5	0.1853490449	0.1857856858	1	0.18734738816	0.1879012404
1	0.1774156943	0.1775242935	1.5	0.17729267679	0.1774430913
1.5	0.1660363999	0.1661157849	2	0.16666477381	0.1662916251

Table 12: The convergent of $\frac{d\mathcal{Y}(0)}{d\xi}$ between DTM and BVP4c.

Ra	BVP4c	DTM	Pr	BVP4c	DTM
0.1	0.1711028535	0.1711093849	0.71	0.14862861147	0.1481786244
0.5	0.1675323832	0.1673885926	2	0.16042257660	0.1609521259
1.5	0.1630022219	0.1637373049	4	0.16801051143	0.1690962489

Table 13: The convergent of $\frac{d\Phi(0)}{d\xi}$ between DTM and BVP4c.

M	BVP4c	DTM	Re	BVP4c	DTM
0.5	-0.800930148	-0.8008846959	1	-0.7848177673	-0.7849803459
1	-0.800930148	-0.8013382819	1.5	-0.6912109272	-0.6915444953
1.5	-0.800734602	-0.803259159	2	-0.6060999399	-0.6068146285

Table 14: The convergent of $\frac{d\Phi(0)}{d\xi}$ between DTM and BVP4c.

Ra	BVP4c	DTM	Pr	BVP4c	DTM
0.1	-0.6018108022	-0.6016038308	0.71	-0.6037313457	-0.6033277469
0.5	-0.7130593437	-0.7134758018	2	-0.2108081003	-0.2108138614
1.5	-0.8323107035	-0.8325678692	4	-0.0418339214	-0.0419023348

Table 15: The convergence of values Π and Λ.

Approximate Order	$Re = 1.5, \Omega = 1, W_e = 0.5, G_r = 1, M = 3,$ $R_a = 0.5, Pr = 2, E_c = 0.5$ and $\varepsilon = \frac{\pi}{6}$		$Re = 1.5, \Omega = 1, W_e = 1, G_r = 1, M = 2,$ $R_a = 0.5, Pr = 3, E_c = 0.5$ and $\varepsilon = \frac{\pi}{6}$	
	Π	Λ	Π	Λ
Order1	0.0000000000	-1.000000000	0.0000000000	-1.0000000000
Order2	-3.331531822	0.2430547952	0.2913252597	-0.3913339011
Order3	0.3878530347	-0.5262507242	0.2252604167	-0.3790444981
Order4	0.4065859693	-0.5034448357	0.2569408256	-0.2866375901
Order5	0.4139701823	-0.4952525053	0.2565293076	-0.2921716017

Table 16: The convergence of values Π and Λ.

Approximate Order	$Re = 1.5, \Omega = 0.1, W_e = 1, G_r = 1, M = 0.5$ $R_a = 0.2, Pr = 0.8, E_c = 0.5$ and $\varepsilon = \frac{\pi}{6}$		$Re = 1, \Omega = 0.1, W_e = 1, G_r = 1, M = 0.75,$ $R_a = 0.1, Pr = 1, E_c = 0.5$ and $\varepsilon = \frac{\pi}{6}$	
	Π	Λ	Π	Λ
Order1	0.0000000000	-1.00000000000	0.00000000000	-1.00000000000
Order2	-1.907228470	-0.4169093458	0.1836320890	-0.6324463133
Order3	0.1712699789	-0.6139260037	0.1843388330	-0.6193322922
Order4	0.1737228598	-0.6003086815	0.1837228598	-0.6003086815
Order5	0.1742478597	-0.597451459	0.1840221637	-0.6168616742

Table 17: The convergence of values Π and Λ.

Approximate Order	$Re = 1, \Omega = 0.1, W_e = 0.5, G_r = 1, M = 1$ $R_a = 0.2, Pr = 0.8, E_c = 0.$ and $\varepsilon = \frac{\pi}{6}$		$Re = 1.5, \Omega = 0.1, W_e = 1, G_r = 1, M = 0.75,$ $R_a = 0.3, Pr = 0.71, E_c = 0.5$ and $\varepsilon = \frac{\pi}{6}$	
	Π	Λ	Π	Λ
Order1	0.0000000000	-1.00000000000	0.0000000000	-1.0000000000
Order2	0.1881176589	-0.7708963375	0.1572284704	-0.7184033024
Order3	0.1854431955	-0.747934427	0.1661351800	-0.6743590811
Order4	0.1849057364	-0.7413847967	0.1683161472	-0.6652208239
Order5	0.1843398768	-0.7407639248	0.1688642291	-0.6636336061

Table 18: The comparison of Exact, Bvp4c and DTM solutions at $W_e = 0$, $G_r = 0$ and $M = 0$.

ξ	$R_e = 1.5$ and $\Omega = 1.2$			$R_e = 2$ and $\Omega = 0.5$		
	Exact	**Bvp4c**	**DTM**	*Exact*	**Bvp4c**	**DTM**
0.1	0.0428147741	0.0428147519	0.04260025998	0.01783948923	0.01633738218	0.01616744682
0.2	0.0796117054	0.0796116618	0.0791481976	0.03317154395	0.03075612657	0.03037957448
0.3	0.1094169011	0.1094168377	0.1086664266	0.04559037548	0.04283090397	0.04220553194
0.4	0.1310988584	0.1310987784	0.1300254678	0.05462452433	0.05204510707	0.05112510641
0.5	0.1433429592	0.1433428673	0.1419262018	0.05972623302	0.05776429978	0.05651595748
0.6	0.1446218357	0.1446217379	0.1428823180	0.06025909824	0.05921462481	0.05764085111
0.7	0.1331609387	0.1331608439	0.1312027677	0.05548372446	0.05545105393	0.05363489368
0.8	0.1068985366	0.1068984565	0.1049742124	0.04454105691	0.04532269275	0.04349276603
0.9	0.0634392391	0.0634391891	0.0620434770	0.02643301632	0.02741393507	0.02605595755
1.0	0.0000000000	0.0000000000	0.0000000000	0.00000000000	0.000000000000	0.00000000000

8 1. The Field of the Velocity

This section highlights the influence of the physical parameters such as the inclination angle, the Prandtl number (P_r), the Weissenberg number (W_e), magnetic field (M), the radiation parameter (R_a), Reynolds number (R_e), and the Grashof number (G_r) on the velocity profile. The effect of the inclination angle on fluid velocity is seen in **Figure (3)**. This figure shows fluid velocity increases with the angle_of inclination is increased. This velocity leads to rising forces acting on the fluid flow. In **Figure (4)** rising trend is noticed for the velocity profile as the Prandtl number increases. The Weissenberg number relative velocity profile is shown in **Figure (5)** presents the relationship between the Weissenberg number and the velocity profile. There is a noticeable upward trend in the bottom wall of the channel, accompanied by a decrease in fluid velocity towards the upper wall. The velocity of the fluid exhibits an increase as the Weissenberg number grows at the lower wall, which can be attributed to the shear-thinning effect. Conversely, the reduction in velocity at the upper wall can be attributed to the increased viscosity of the non-Newtonian fluid. The phenomenon of shear thinning is a distinctive characteristic shown by the Williamson fluid. The fluid under consideration exhibits the characteristic of being a non-Newtonian fluid, wherein its viscosity diminishes as the applied shear stress increases. Furthermore, the Williamson fluid parameter quantifies the impact of viscosity on elasticity. As a result, a decrease in the velocity profile occurs as a consequence of the reduced resistance to flow. **Figure (6)** shows how a fluid velocity responds to the effect of an external magnetic field. It shows that fluid velocity experiences a loss of momentum. This is predicted because the used magnetic field Lorentz force creates a resistive force within the flow, which slows the Williamson fluid velocity. It is also noteworthy that the velocity boundary layers thickness reduces as M value increases. **Figure (7)** indicates an increase in fluid velocity as the value of the radiation parameter is decreased. This observation indicates an increase in the thickness of the boundary layer, which causes more fluid flow. **Figure (8)** explains the velocity response to changes in Reynolds number. It has been observed that fluid velocity decreases as Reynolds number increases. This assertion is valid from a physical standpoint, as the Reynolds number serves as an indicator of the relative importance of inertial effects compared to viscous effects. Because of this, fluid velocity slows down as seen in the image. **Figure (9)** displays that the fluid velocity rises when the Grashof number is raised.

8.2   The Field of the Temperature

The Sketches the behavior of the field temperature for different values of the inclination angle parameter (ε), radiation parameter (R_a), magnetic field parameter (M), Reynolds number (R_e) Ekartl number (E_c), Weissenberg number (W_e), and the Prandtl number (P_r) shown in **Figures (10–16)**.

In general, the increasing values of each of the parameters increase fluid temperature except the value of radiation parameter for which the opposite occurs. The effect of the angle of inclination parameter is shown in relation to fluid temperature in **Figure (10)**. The fluid temperature looks to have slightly increased as the parameter fluctuates. This is because increased fluid velocity, as seen in **Figure (3)**, tends to increase the forces acting on fluid flow, increasing fluid temperature. **Figure (11)** shows an increasing trend in fluid temperature for growing radiation parameter values. This is explained by the fact that reducing the fluid's Rosseland the absorption parameter $(\bar{\tau}^c)$ while raising the parameter radiation decreases the fluid's temperature. It is shown in **Figure (12)** how the magnetic field parameter affects fluid temperature. As M's value increases, the temperature is shown to be increasing as well. An electrically conducting fluid will interact with a magnetic field when it is applied, creating the Lorentz force. The Lorentz force slows fluid motion, causing the

kinetic energy to be transformed to heat energy (Joule heating), which increases the fluid's temperature. The relationship between Reynolds number and fluid temperature is seen in Figure (13), indicating a positive correlation as Reynolds number increases. The observed phenomenon can be ascribed to an augmentation in frictional force, which in turn enhances the thermal dispersion of the fluid, resulting in an elevation of the fluid's temperature. **Figure (14)- Figure (16)** demonstrate that the temperature profile rises with increasing the values of E_c, W_e and P_r.
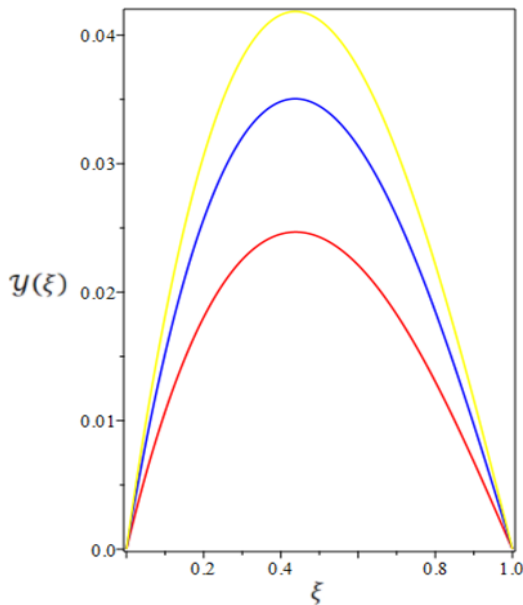
Figure 3: ε vs Velocity Profile, when $G_r = 1, R_a = 0.3, P_r = 3, M = 2, R_e = 1.5,$ $\Omega = 1 , E_c = 0.5$ and $W_e = 0.5.$
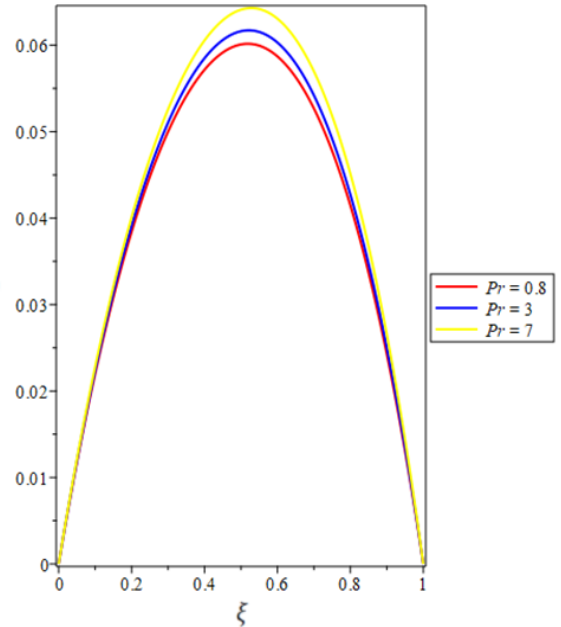
Figure 4: Pr vs Velocity Profile, when $G_r = 1, R_a = 0.3, M = 3, W_e = 0.5, R_e = 1,$ $\Omega = 1 , E_c = 0.5$ and $\varepsilon = \frac{\pi}{6}.$
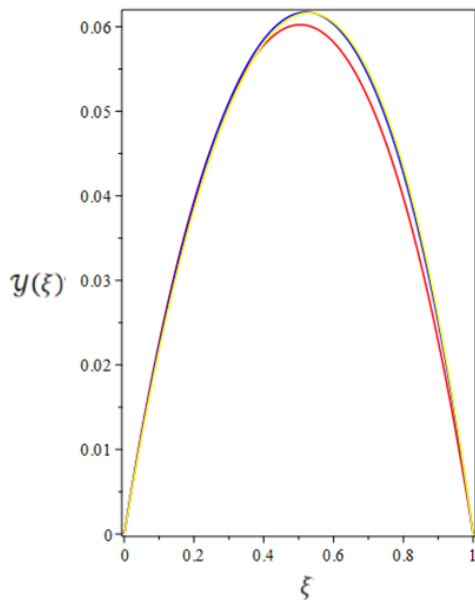
Figure 5: W_e vs Velocity Profile, when $G_r = 1, R_a = 0.3, P_r = 3, M = 3$ $R_e = 1.5, \Omega = 1 , E_c = 0.5$ and $\varepsilon = \frac{\pi}{6}.$
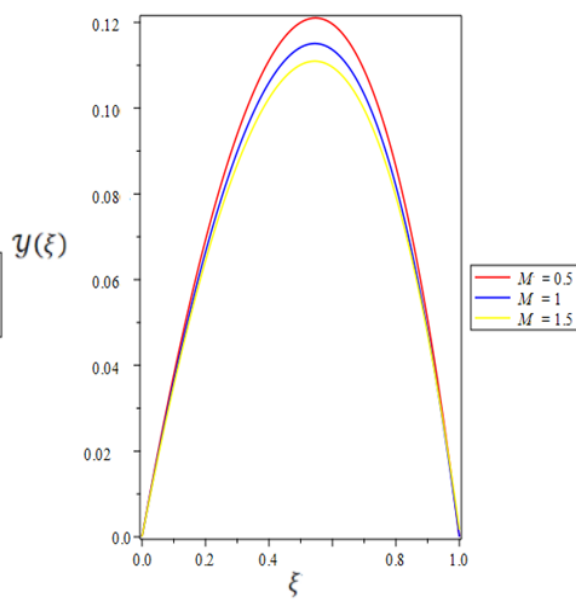
Figure 6: M vs Velocity Profile, when $G_r = 1, R_a = 0.3, P_r = 2, W_e = 0.5,$ $R_e = 1, \Omega = 1 , E_c = 0.5$ and $\varepsilon = \frac{\pi}{6}.$
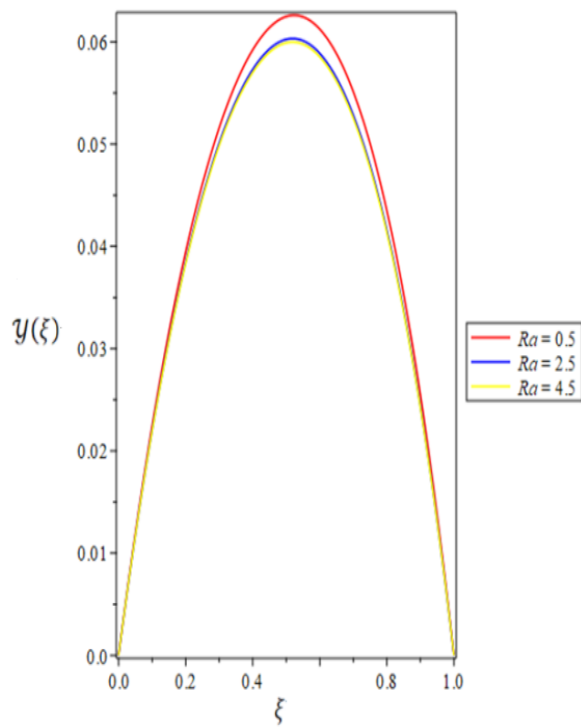
Figure 7: Ra versus Velocity Profile, when $G_r = 1, \mathrm{R}_e = 0.5, \mathrm{P}_r = 2, \mathrm{M} = 3, \mathrm{W}_e = 0.1,$ $\Omega = 1, \mathrm{E}_c = 0.5$ and $= \frac{\pi}{6}$.
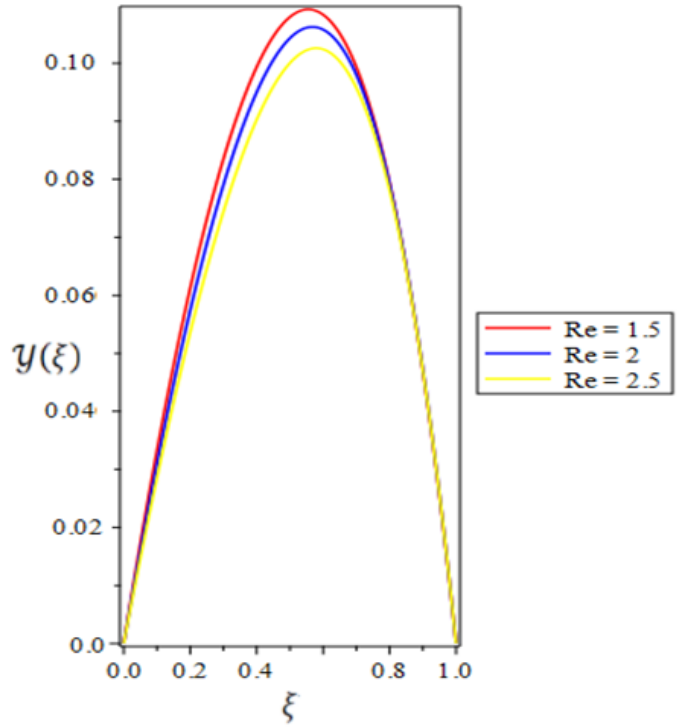
Figure 8: Re vs Velocity Profile, when $G_r = 1, \mathrm{R}_a = 0.3, \mathrm{P}_r = 2, \mathrm{W}_e = 0.5,$ $\Omega = 1, \mathrm{E}_c = 0.5$ and $\varepsilon = \frac{\pi}{6}$.
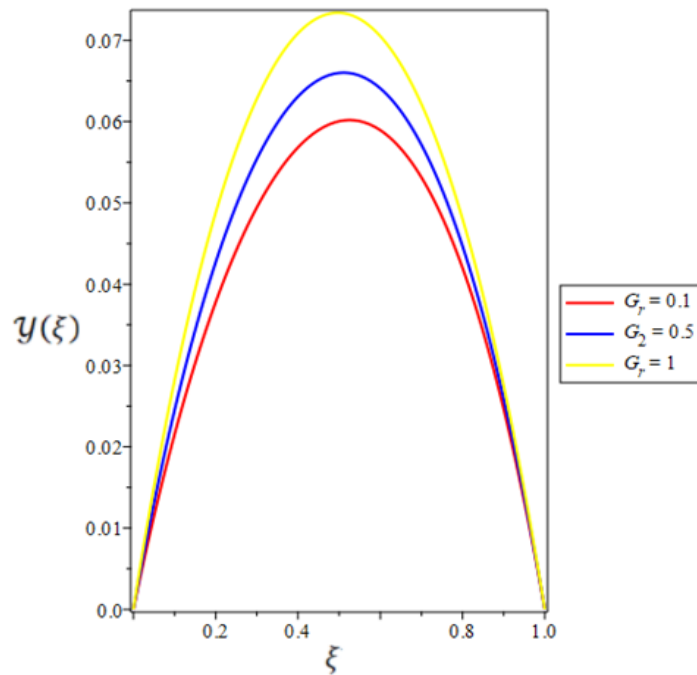
Figure.9: G_r versus Velocity Profile, when $\mathrm{R}_a = 0.5, \mathrm{R}_e = 1.5, \mathrm{P}_r = 2, \mathrm{M} = 3, \mathrm{W}_e = 0.5,$ $\Omega = 1, \mathrm{E}_c = 0.5$ and $\varepsilon = \frac{\pi}{6}$.
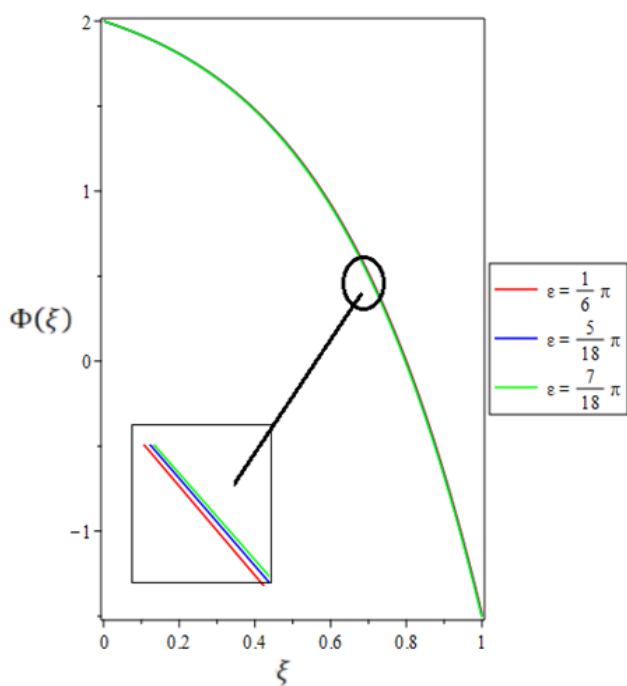
Figure 10: ε vs Temperature Profile, when $G_r = 1, R_e = 1.5, P_r = 3, M = 3,$ $W_e = 0.5, \Omega = 1 , E_c = 0.5$ and $R_a = 0.5.$
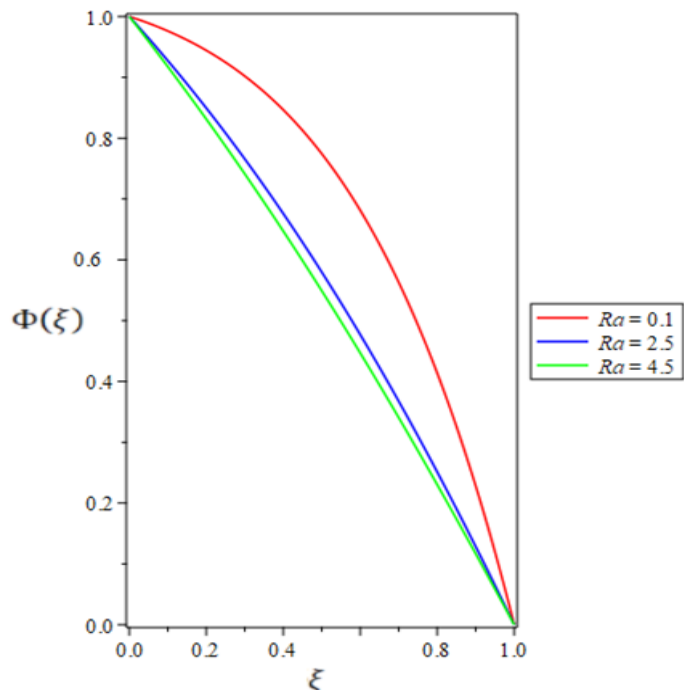
Figure 11: R_a vs Temperature Profile, when $G_r = 1, R_e = 1.5, P_r = 2, W_e = 0.5,$ $M = 3, \Omega = 1 , E_c = 0.5$ and $\varepsilon = \frac{\pi}{6}.$
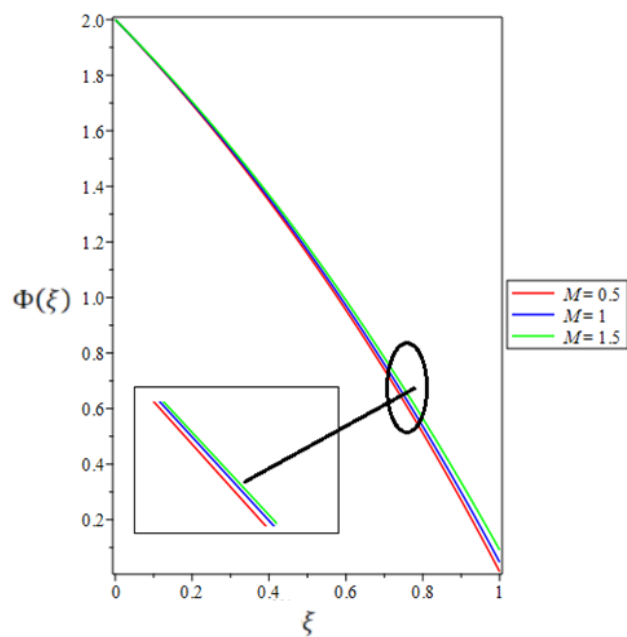
Figure 12: *M* vs Temperature Profile, when $G_r = 1, R_e = 1.5, P_r = 2, R_a = 0.5,$ $W_e = 0.3, \Omega = 1 , E_c = 0.5$ and $\varepsilon = \frac{\pi}{6}.$
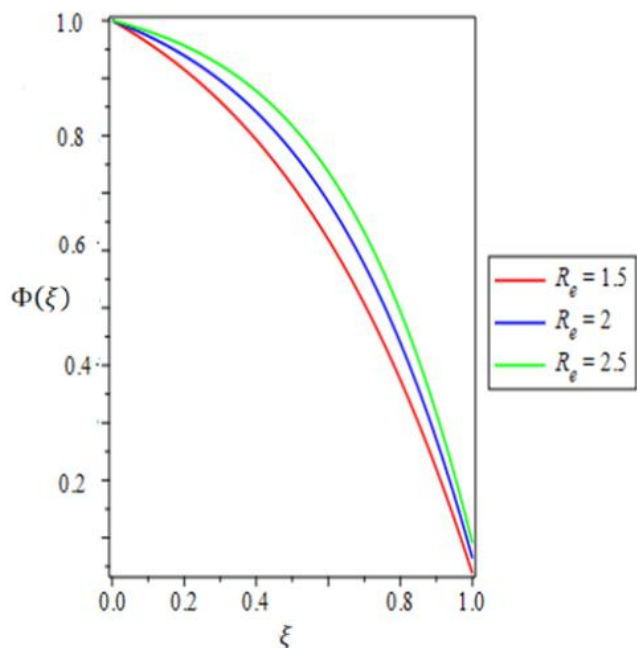
Figure 13: R_e vs Temperature Profile, when $G_r = 1, R_a = 0.5, P_r = 3, W_e = 0.5,$ $M = 2, \Omega = 1 , E_c = 0.5$ and $\varepsilon = \frac{\pi}{6}.$
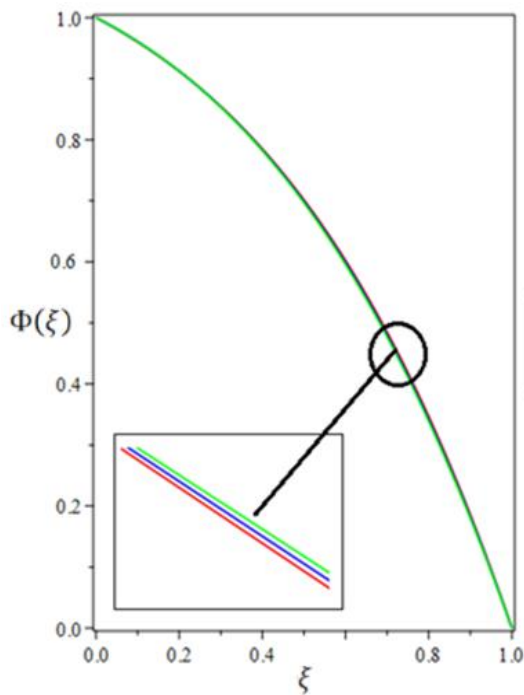
Figure 14: E_c vs Temperature Profile, when $G_r = 1, R_e = 1.5, P_r = 2, R_a = 0.5,$ $W_e = 0.3, \Omega = 1, M = 3$ and $\varepsilon = \frac{\pi}{6}$.
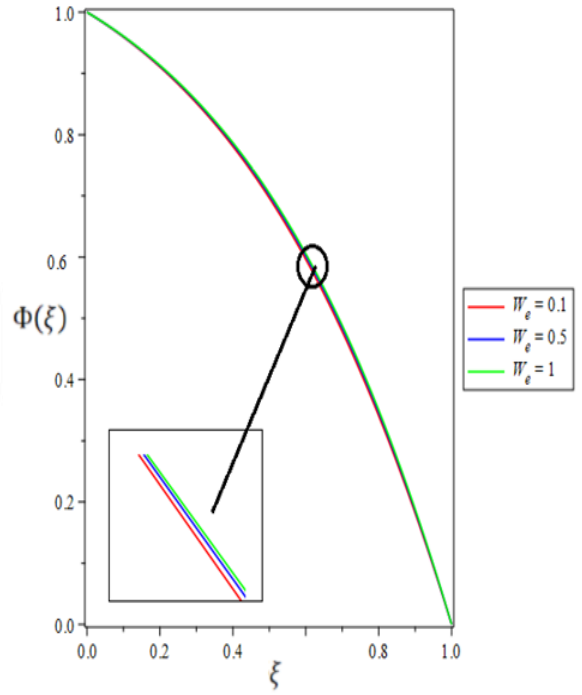
Figure 15: W_e vs Temperature Profile, when $G_r = 1, R_e = 1.5, P_r = 3, M = 2,$ $R_a = 0.5, \Omega = 1, E_c = 0.5$ and $\varepsilon = \frac{\pi}{6}$.
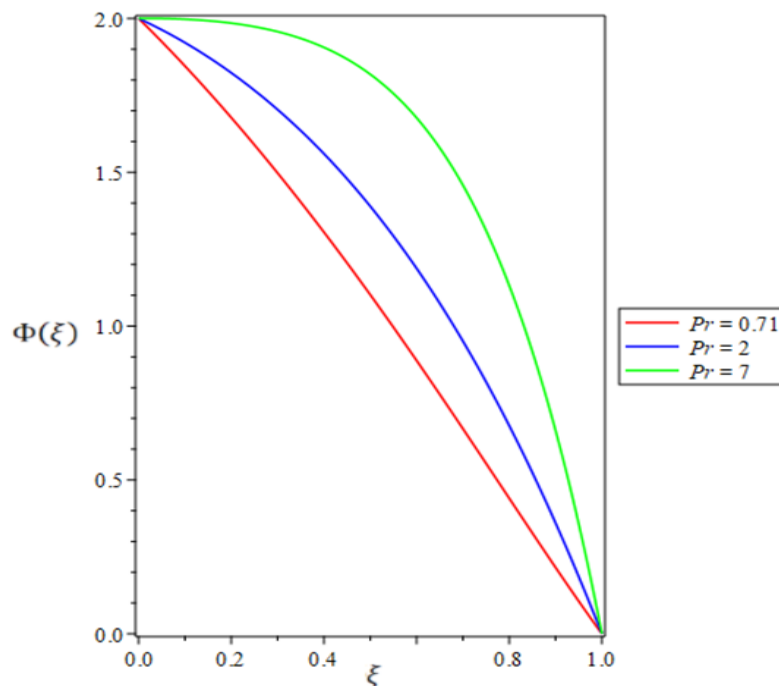
Figure 16: P_r vs Temperature Profile, when $G_r = 1, R_e = 1.5, E_c = 0.5, R_a = 0.5, W_e = 0.5, \Omega = 1,$ $M = 3$ and $\varepsilon = \frac{\pi}{6}$.

8.3 The Graphic results of Bejan number and entropy Generation.

Figures (17–21) show how different controlling parameters affect the development of entropy inside the channel. According to **Figure (17)**, fluid entropy production increases at the lower wall and reduces at the higher wall when the angle in the inclination parameter

increases. The rise at the lower wall is due to the forces acting on the fluid flow being increased by higher fluid velocity, which causes more entropy to develop.

Figure (18), shows how the Weissenberg number (W_e) affects the production of fluid entropy. Entropy generation is reduced as W_e grows, but only somewhat so near the upper wall of the channel. This is caused by the shear-thinning effect, which, as stated in **Figure (4)**, results in decreased flow velocity at the lower wall. Entropy generation is shown to be decreasing in **Figure (19)** for the magnetic field increase. **Figure (20) and Figure (20)** proved the effect of the Reynolds number and the Prandtl number on the fluid temperature respectively. These figures displayed entropy generation is greatly reduced at the lower channel but concedes to a strong surge at the upper channel.

The Bejan number response to changes in the angle of inclination parameter, Reynolds number, Prandtl number, radiation parameter, Weissenberg number and magnetic field parameter is shown in **Figures (22)-(27)**. As the angle of inclination parameter grows in value in **Figure (22)**, the Bejan number drops at the bottom wall, making it clear that fluid friction predominates entropy formation. According to Weissenberg number, heat transfer predominates at both the middle and upper walls, whereas the friction of fluid is effective at causing entropy production at the bottom wall, as shown in **Figure (23)**. **Figure (24)** shows that the main source of entropy generation is heat transfer since Bejan number values rise as the magnetic field parameter rises over the whole channel. On the other hand, **Figure (25)** represents a change in the pattern since entropy generation drops as Reynolds number increases. **Figure (26)** shows that as the radiation parameter rises, heat transfer takes precedence over entropy generation. However, **Figure (27)** displays the Bejan number rising with an increase in the Prandtl parameter.
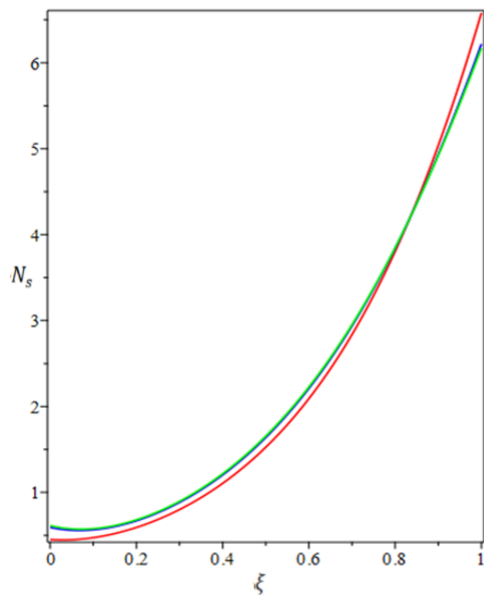
Figure 17: ε vs Entropy Generation, when $G_r = 1, R_e = 1, P_r = 3, R_a = 0.5, W_e = 0.5$ $\Omega = 1$, $M = 2$ and $E_c = 0.5$.
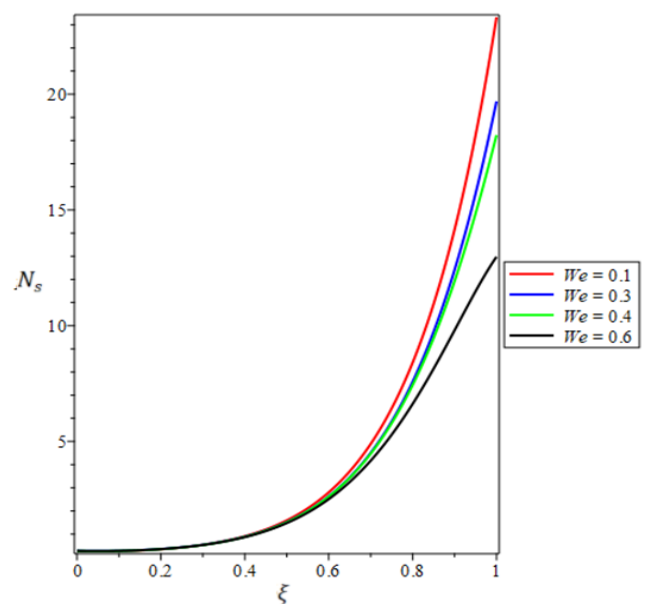
Figure 18: We vs Entropy Generation, when $G_r = 1, R_a = 0.5, P_r = 3, R_e = 1,$ $M = 2, \Omega = 1$, $E_c = 0.5$ and $\varepsilon = \frac{\pi}{6}$.
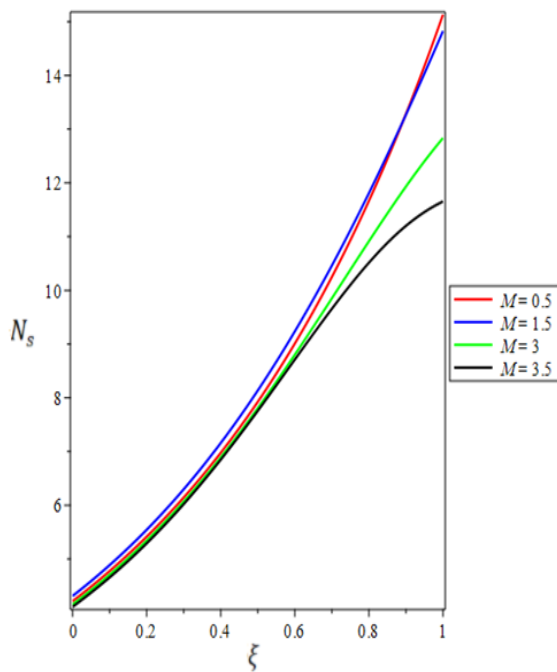
Figure 19: M vs Entropy Generation, when $G_r = 1, \mathrm{R}_e = 1, \mathrm{P}_r = 3, \mathrm{R}_a = 0.5,$ $\mathrm{W}_e = 0.5, \Omega = 1, \mathrm{E}_c = 0.5$ and $\varepsilon = \frac{\pi}{6}$.
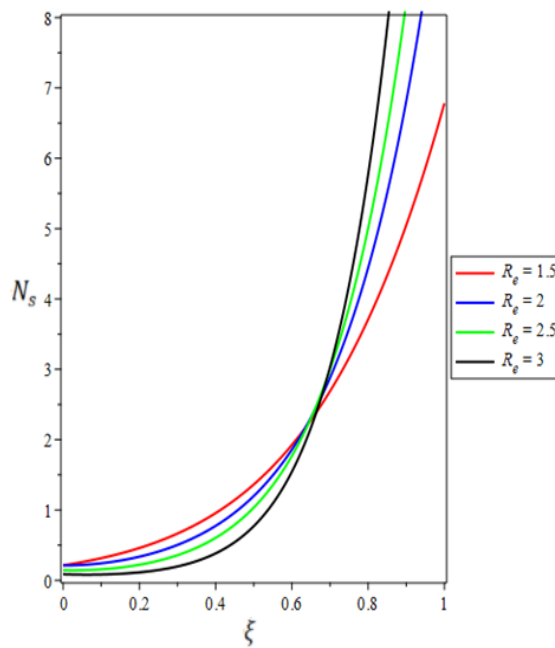
Figure 20: R_e vs Entropy Generation, when $G_r = 1, \mathrm{R}_a = 0.5, \mathrm{P}_r = 2, We = 0.5,$ $\mathrm{M} = 3, \Omega = 1, \mathrm{E}_c = 0.5$ and $\varepsilon = \frac{\pi}{6}$.
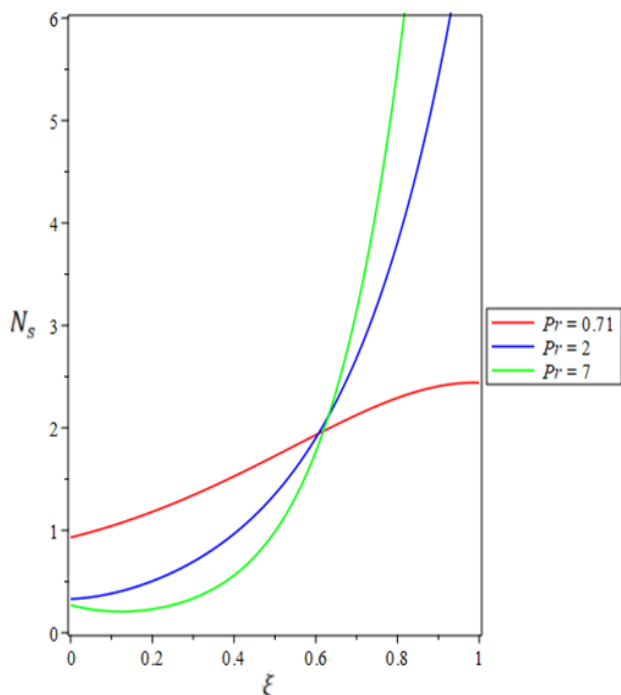
Figure 21: Pr vs Entropy Generation, when $G_r = 1, \mathrm{R}_e = 1, M = 3, \mathrm{R}_a = 0.5$ $\mathrm{W}_e = 0.5, \Omega = 1, \mathrm{E}_c = 0.5$ and $\varepsilon = \frac{\pi}{6}$.
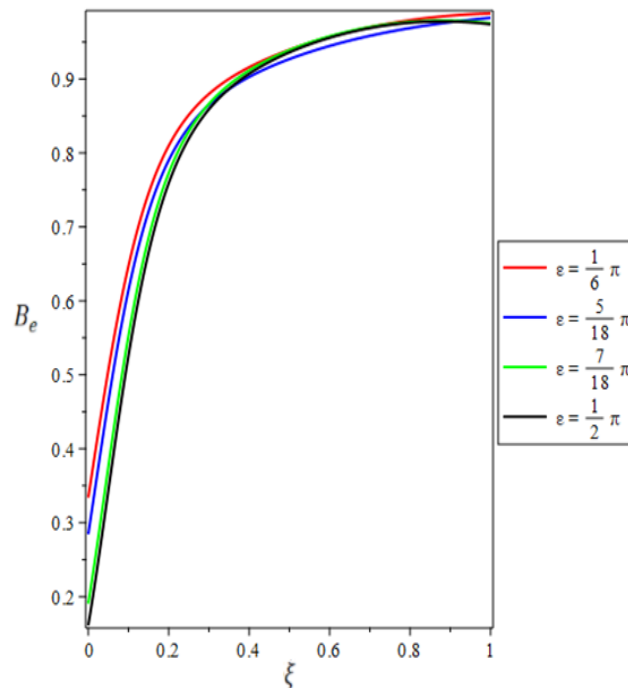
Figure 22: ε vs Bejan number, when $G_r = 1, \mathrm{R}_e = 1, \mathrm{P}_r = 4, \mathrm{R}_a = 0.5,$ $\mathrm{W}_e = 0.5, \Omega = 1, \mathrm{E}_c = 1$ and $M = 3$.
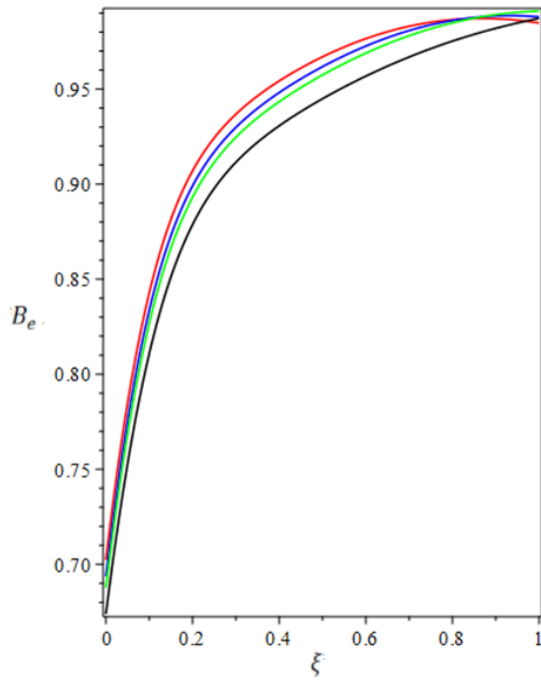
Figure 23: W_e vs Bejan number, when $G_r = 1, R_a = 0.5, P_r = 3, R_e = 1.5,$ $M = 2, \Omega = 1, E_c = 1$ and $= \frac{\pi}{6}$.
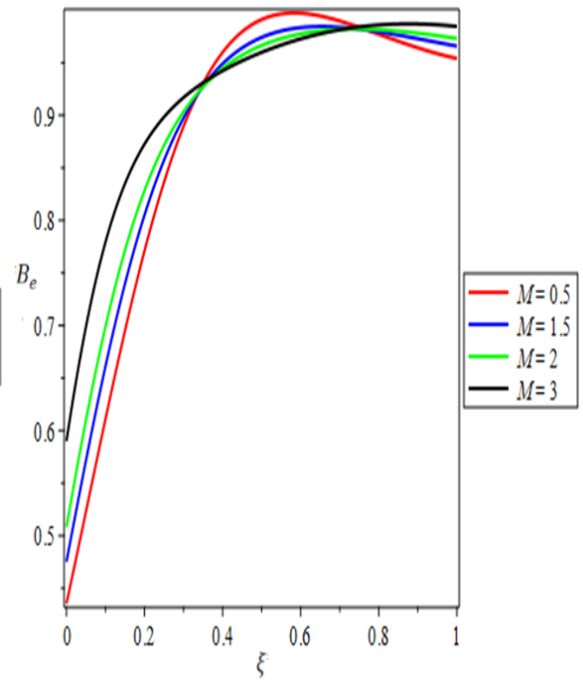
Figure 24: M vs Bejan number, when $G_r = 1, R_e = 1.5, P_r = 2, R_a = 0.5,$ $W_e = 0.5, \Omega = 1, E_c = 1$ and $\varepsilon = \frac{\pi}{6}$.
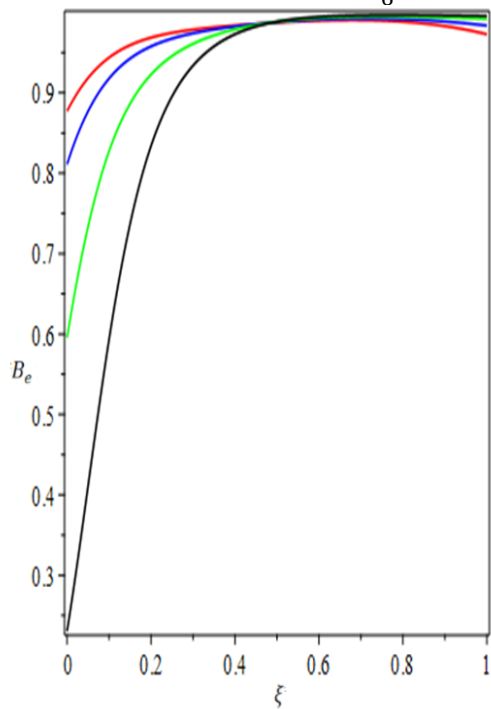
Figure 25: R_e vs Bejan number, when $G_r = 1, R_a = 0.5, P_r = 3, R_e = 1.5,$ $M = 2, \Omega = 1, E_c = 1$ and $\varepsilon = \frac{\pi}{6}$.
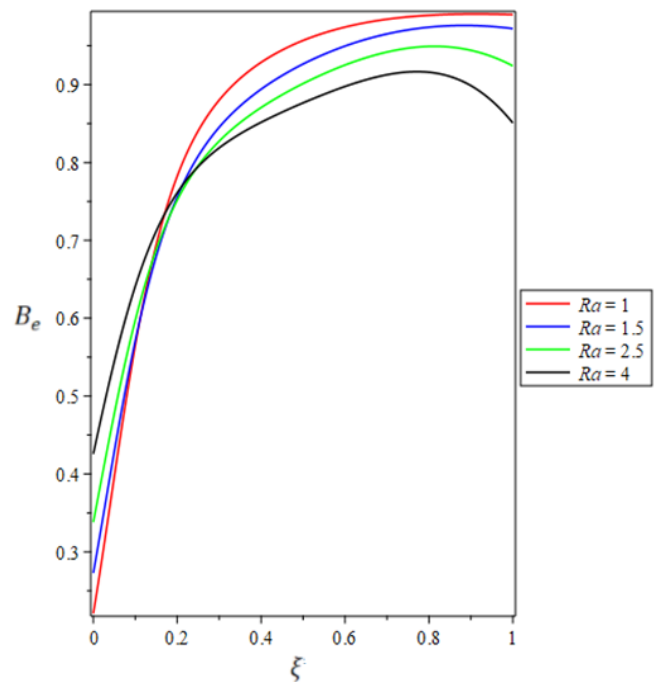
Figure 26: Ra vs Bejan number, when $G_r = 1, R_e = 1, P_r = 2, M = 2, W_e = 0.5,$ $\Omega = 1, E_c = 0.5$ and $\varepsilon = \frac{\pi}{6}$.
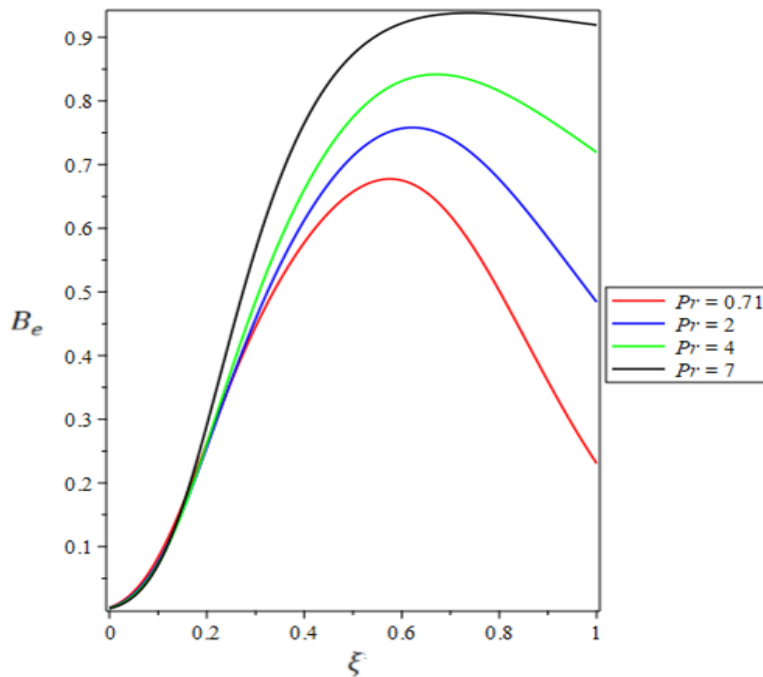
Figure 27: Pr vs Bejan number, when $G_r = 1, \mathrm{R}_a = 0.5,$ $\mathrm{We} = 0.5$, $\mathrm{R}_e = 1.5, \mathrm{M} = 3, \Omega = 1$, $\mathrm{E}_c = 0.5$ and $= \frac{\pi}{6}$.

9. Conclusions

This study investigates the heat irreversibility analysis of thermal radiation, Ohmic heating, and angle of inclination on Williamson fluid. The derived flow model equations are solved using the differential transform method and bvp4c. Plots show the flow characteristics for the velocity, temperature, entropy generation, and Bejan number. The entropy generation and Bejan number are examined using the data for the velocity and temperature profiles. It also shows us that flow motion is reduced by the magnetic field parameter, Reynolds number, and the radiation parameter whereas fluid velocity is increased by the angle of inclination parameter and Prandtl number, with his note, the fluid temperature is increased by the angle of inclination, the magnetic parameter, and the Reynold number. We got that the radiation coefficient is the only variable that hinders the production of entropy at the upper wall. It also turns out that fluid friction dominates the formation of entropy with increasing levels, the slope coefficient, the Weissenberg number, the Reynolds number, and the radiation parameter, while the magnetic field coefficient and the Prandtl number show the dominance of thermal irreversibility.

References
[1] R. V. Williamson, "The flow of pseudoplastic materials," *Ind. Eng. Chem.*, vol. 21, no. 11, pp. 1108–1111, 1929.
[2] M. Ijaz Khan and F. Alzahrani, "Activation energy and binary chemical reaction effect in nonlinear thermal radiative stagnation point flow of Walter-B nanofluid: Numerical computations," Int. J. Mod. Phys. B, vol. 34, no. 13, pp. 2050132, 2020.
[3] S. Nadeem, S. T. Hussain, and C. Lee, "Flow of a Williamson fluid over a stretching sheet," Braz. J. Chem. Eng., vol. 30, no. 3, pp. 619–625, 2013.
[4] T. Hayat, A. Shafiq, and A. Alsaedi, "Hydromagnetic boundary layer flow of Williamson fluid in the presence of thermal radiation and Ohmic dissipation," Alex. Eng. J., vol. 55, no. 3, pp. 2229–2240, 2016.

[5] M. R. Krishnamurthy, B. C. Prasannakumara, B. J. Gireesha, and R. S. R. Gorla, "Effect of chemical reaction on MHD boundary layer flow and melting heat transfer of Williamson nanofluid in porous medium," Eng. Sci. Technol. Int. J., vol. 19, no. 1, pp. 53–61, 2016.

[6] J. Raza, F. Mebarek-Oudina, and B. Mahanthesh, "Magnetohydrodynamic flow of nano Williamson fluid generated by stretching plate with multiple slips," Multidiscip. Model. Mater. Struct., vol. 15, no. 5, pp. 871–894, 2019.

[7] M. Y. Malik, T. Salahuddin, A. Hussain, S. Bilal, and M. Awais, "Homogeneous-heterogeneous reactions in Williamson fluid model over a stretching cylinder by using Keller box method," AIP Adv., vol. 5, no. 10, p. 107227, 2015.

[8] D. Al-Khafajy and W. N. Al-Delfi, "The Peristaltic Flow of Williamson Fluid through a Flexible Channel," *Iraqi Journal of Science*, pp. 865–877, 2023.

[9] M. Monica, J. Sucharitha, and C. Kumar, "Stagnation point flow of a Williamson fluid over a nonlinearly stretching sheet with thermal radiation," Am. Chem. Sci. J., vol. 13, no. 4, pp. 1–8, 2016.

[10] L. Nagaraja, M. S. Reddy, and M. S. Reddy, "Heat transfer of non-Newtonian Williamson fluid flow past a circular cylinder with suction and injection," Int. j. of Innovative Research in Sci. & Tech, vol. 6, pp. 48–54, 2017.

[11] W. Khudair and D. G. Sadiq, "Influence of heat transfer on MHD oscillatory flow for Williamson fluid with variable viscosity through a porous medium," *Int. J. Fluid Mechanics & Thermal Sciences*, vol. 4, no. 1, pp. 11–17, 2018.

[12] A. M. Siddiqui, S. Bhatti, M. A. Rana, and M. Zahid, "Blade coating analysis of a Williamson fluid," Results Phys., vol. 7, pp. 2845–2850, 2017.

[13] D. G. Al-Khafajy, "Influence of MHD and Wall Properties on the Peristaltic Transport of a Williamson Fluid with Variable Viscosity Through Porous Medium," *Iraqi Journal of Sciences*, pp. 1076–1089, 2017.

[14] S. N S, M. Macha, S. S, G. B J, and K. Naikoti, "Thermal analysis of MHD Williamson fluid flow through a microchannel," *Int. Commun. Heat Mass Transf.*, vol. 127, no. 105582, p. 105582, 2021.

[15] B. M. J. Rana et al., "Swimming of microbes in blood flow of nano-bioconvective Williamson fluid," Therm. Sci. Eng. Prog., vol. 25, no. 101018, p. 101018, 2021.

[16] B. M. J. Rana, S. M. Arifuzzaman, S. Reza-E-Rabbi, S. F. Ahmed, and M. Shakhaoath Khan, "Energy and magnetic flow analysis of Williamson micropolar nanofluid through stretching sheet," Heat Technol., vol. 37, no. 2, pp. 487–496, 2019.

[17] J. A. Rao, G. Vasumathi, and J. Mounica, "Joule heating and thermal radiation effects on MHD boundary layer flow of a nanofluid over an exponentially stretching sheet in a porous medium," World J. Mech., vol. 05, no. 09, pp. 151–164, 2015.

[18] D. Prakash, "Influence of viscous and Ohmic heating on MHD flow of nanofluid over an inclined nonlinear stretching sheet embedded in a porous medium," International Journal of Mechanical Engineering and Technology (IJMET), vol. 9, pp. 992–1001, 2018

[19] T. Muhammad, T. Hayat, S. A. Shehzad, and A. Alsaedi, "Viscous dissipation and Joule heating effects in MHD 3D flow with heat and mass fluxes," Results Phys., vol. 8, pp. 365–371, 2018.

[20] K. S. Adegbie, D. J. Samuel, and B. O. Ajayi, "Ohmic heating of magnetohydrodynamic viscous flow over a continuous moving plate with viscous dissipation buoyancy and thermal radiation," Defect Diffus. For., vol. 392, pp. 73–91, 2019.

[21] B. Shankar Goud and M. M. Nandeppanavar, "Ohmic heating and chemical reaction effect on MHD flow of micropolar fluid past a stretching surface," *Partial Differ. Equ. Appl. Math.*, vol. 4, no. 100104, p. 100104, 2021.

[22] M. M. Hasan, M. A. Samad, and M. M. Hossain, "Effects of hall current and ohmic heating on non-Newtonian fluid flow in a channel due to peristaltic wave," *Appl. Math. (Irvine)*, vol. 11, no. 04, pp. 292–306, 2020.

[23] B. J. Gireesha, K. Ganesh Kumar, M. R. Krishnamurthy, S. Manjunatha, and N. G. Rudraswamy, "Impact of ohmic heating on MHD mixed convection flow of Casson fluid by considering Cross diffusion effect," *Nonlinear Eng.*, vol. 8, no. 1, pp. 380–388, 2019.

[24] D. J. Samuel and B. I. Olajuwon, "Insight into the effects of thermal radiation and Ohmic heating on chemically reactive Maxwell fluid subject to Lorentz force and buoyancy force," *Journal of the Nigerian Mathematical Society*, vol. 41, pp. 27–48, 2022.

[25] A. Bejan, *Convection Heat Transfer*. Chichester, England: John Wiley & Sons, 2013.

[26] S. Saouli and S. Aıboud-Saouli, "Second law analysis of laminar falling liquid film along an inclined heated plate," *International Communications in Heat and Mass Transfer*, vol. 31, pp. 879–886, 2004.

[27] S. O. Adesanya, "Entropy generation analysis for a reactive couple stress fluid flow through a channel saturated with porous material," *Energy*, vol. 93, pp. 1239–1245, 2015.

[28] S. O. Adesanya and O. D. Makinde, "Thermodynamic analysis for a third-grade fluid through a vertical channel with internal heat generation," *Journal of Hydrodynamics*, vol. 27, pp. 264–272, 2015.

[29] S. S. S. Sen, M. Das, R. Mahato, and S. Shaw, "Entropy analysis on nonlinear radiative MHD flow of Diamond-Co3O4/ethylene glycol hybrid nanofluid with catalytic effects," *Int. Commun. Heat Mass Transf.*, vol. 129, no. 105704, p. 105704, 2021.

[30] M. K. Nayak, S. Shaw, M. Ijaz Khan, O. D. Makinde, Y.-M. Chu, and S. U. Khan, "Interfacial layer and shape effects of modified Hamilton's Crosser model in entropy optimized Darcy-Forchheimer flow," *Alex. Eng. J.*, vol. 60, no. 4, pp. 4067–4083, 2021.

[31] A. A. Opanuga, O. O. Agboola, J. A. Gbadeyan, and H. I. Okagbue, "Entropy generation analysis of Hall current effect on MHD micropolar fluid flow with rotation effect," *SN Appl. Sci.*, vol. 2, no. 1, 2020.

[32] A. A. Opanuga, J. A. Gbadeyan, O. O. Agboola, and H. I. Okagbue, "Effect of suction/injection on the entropy generation of third-grade fluid with convective cooling," *Defect Diffus. For.*, vol. 384, pp. 21–30, 2018.

[33] Q. Ni, Z. L. Zhang, and L. Wang, "Application of the differential transformation method to vibration analysis of pipes conveying fluid," *Applied Mathematics and Computation*, vol. 217, pp. 7028–7038, 2011.

[34] B. Kundu, R. Das, and K.-S. Lee, "Differential transform method for thermal analysis of exponential fins under sensible and latent heat transfer," *Procedia Engineering*, vol. 127, pp. 287–294, 2015.

[35] M. Usman, M. Hamid, U. Khan, S. T. Mohyud Din, M. A. Iqbal, and W. Wang, "Differential transform method for unsteady nanofluid flow and heat transfer," *Alex. Eng. J.*, vol. 57, no. 3, pp. 1867–1875, 2018.

[36] K. Jabeen, M. Mushtaq, and R. M. Akram, "A comparative study of MHD flow analysis in a porous medium by using differential transformation method and variational iteration method," *Journal of Contemporary Applied Mathematics*, vol. 9, pp. 1–15, 2019.

[37] N. D. Patel and R. Meher, "Differential transformation method for solving Kolmogrove-Petrovskii-Piskunov equation and porous medium equation," *Mathematical Sciences, IMRF Journals*, vol. 5, pp. 47–51, 2016.

[38] H. Yaghoobi and M. Torabi, "The application of differential transformation method to nonlinear equations arising in heat transfer," *International Communications in Heat and Mass Transfer*, vol. 38, pp. 815–820, 2011.

[39] R. Meher and N. D. Patel, "Analytical Investigation of MHD Jeffery-Hamel flow problem with heat transfer by differential transform method," *SN Applied Sciences*, vol. 1, pp. 1–12, 2019.

[40] N. Patel and R. Meher, "Analytical investigation of Jeffery-Hemal flow with magnetic field by differential transform method," *Int. J. Adv. Appl. Math. Mech*, vol. 6, pp. 1–9, 2018.

[41] O. Makinde and A. Daniel, "Effects of convective heating on entropy generation rate in a channel with permeable walls," *Entropy*, vol. 15, pp. 220–233, 2013.